THE ROLE OF NICKEL SURFACE CURVATURE IN THE HIGH-TEMPERATURE OXIDATION OF NICKEL 270

By

H. JOHN HEALEY, JR.

A DISSERTATION PRESENTED TO THE GRADUATE COUNCIL OF
THE UNIVERSITY OF FLORIDA
IN PARTIAL FULFILLMENT OF THE REQUIREMENTS FOR THE
DEGREE OF DOCTOR OF PHILOSOPHY

UNIVERSITY OF FLORIDA

JUNE 1978

Copyright by
H. John Healey, Jr.
1978

To my parents and Dianne

ACKNOWLEDGEMENTS

The author wishes to express his gratitude to the members of his supervisory committee, Drs. F. N. Rhines, R. T. DeHoff, E. D. Verink, Jr. and J. E. Keesling, for their service on the committee and their guidance in the research. In particular, the author wishes to thank Drs. F. N. Rhines and R. G. Connell, Jr., for their many discussions concerning the mechanism of the high-temperature oxidation of nickel. The laboratory assistance of P. V. Malone and N. H. Slater proved very helpful and is hereby acknowledged.

It is with gratitude that the author acknowledges the financial support of the National Science Foundation, under whose sponsorship this research was conducted. Special thanks go to Huntington Alloys, Inc., Huntington, West Virginia, and to the Francis L. LaQue Laboratory, Wrightsville Beach, North Carolina, for supplying the Nickel 270 used in the research.

TABLE OF CONTENTS

Page

ACKNOWLEDGEMENTS....iv

LIST OF TABLES....vii

LIST OF FIGURES....ix

ABSTRACT....xiii

CHAPTER

I INTRODUCTION....1

1.1. The Scientific Background for the Research....2
1.2. The Objective of the Research....16

II EXPERIMENTAL TECHNIQUES....18

2.1. Specimen Preparation....18
2.2. Oxidation....19
2.3. Metallographic Preparation....23
2.4. Scale Thickness Measurements....23
2.5. Determination of Mean Grain Intercept...26

III EXPERIMENTAL RESULTS....29

3.1. Growth of NiO Upon Curved Specimens....29
3.2. Growth of NiO Upon Flat Specimens....65

IV DISCUSSION OF THE EXPERIMENTAL RESULTS....96

4.1. The Effect of Nickel Surface Curvature Upon the High-Temperature Oxidation of Nickel....98
4.2. The Effect of Oxidation Temperature Upon the High-Temperature Oxidation of Nickel....131

V CONCLUSIONS....137

TABLE OF CONTENTS - Continued

Page

APPENDIX

I EQUIAXED LAYER THICKNESS DATA FOR WIRE, HOLE AND FLAT SPECIMENS.....140

II COMPUTATION OF THE "CALCULATED" TOTAL SCALE THICKNESS FOR THE NiO FORMED UPON CURVED SPECIMENS.....144

BIBLIOGRAPHY.....147

BIOGRAPHICAL SKETCH.....153

LIST OF TABLES

Table		Page
I	Standardized Surface Preparation for Nickel 270 Specimens	20
II	Metallographic Procedures	24
III	Total NiO Scale Thickness Measurements for Wire and Hole Nickel 270 Specimens	36
IV	Mean Values of the Number of NiO Grain Boundary Intercepts for the Columnar and Equiaxed Layers of the Scale Formed Upon Wire and Hole Nickel 270 Specimens	47
V	Mean Grain Intercept Values for the Columnar and Equiaxed Layers of the Scale Formed Upon Wire and Hole Nickel 270 Specimens	50
VI	Equiaxed Fraction of the Total Scale Thickness for Wire and Hole Nickel 270 Specimens	53
VII	Columnarity Values of the Outer Layer of NiO Formed Upon Wire and Hole Nickel 270 Specimens	66
VIII	Columnar Layer Thickness Measurements for Wire and Hole Nickel 270 Specimens	75
IX	Total NiO Scale Thickness Measurements for Flat Nickel 270 Specimens	87
X	Equiaxed Fraction of the Total Scale Thickness for Flat Nickel 270 Specimens	90
XI	Columnar Layer Thickness Measurements for Flat Nickel 270 Specimens	93
XII	Incubation Times for NiO Grown Upon Wire and Hole Nickel 270 Specimens Calculated From Total Scale Thickness Data	105

LIST OF TABLES - Continued

Table		Page
XIII	Incubation Times for NiO Grown Upon Wire and Hole Nickel 270 Specimens Calculated From Columnar Layer Thickness Data	106
XIV	NiO Grain Boundary Surface Area Per Unit Volume of Scale for Wire and Hole Nickel 270 Specimens	110
XV	Radius of the Metal/Oxide Interface for Wire and Hole Nickel 270 Specimens	120
XVI	Incubation Times for NiO Grown Upon Flat Nickel 270 Specimens Calculated From Total Scale Thickness Data	133
XVII	Incubation Times for NiO Grown Upon Flat Nicle 270 Specimens Calculated From Columnar Layer Thickness Data	134

LIST OF FIGURES

Figure		Page
1	Microstructure of NiO scale formed upon a flat specimen under pure oxygen at one atmosphere of pressure for 49 hours at 1000°C	4
2	Schematic diagram of the oxidation system used for oxidizing the Nickel 270 specimens	21
3	Test line orientation for determining the number of NiO grain boundary intercepts in the columnar and equiaxed layers,	
	(a) NiO formed upon wire specimens	27
	(b) NiO formed upon hole specimens	27
4	Microstructure of NiO scale formed upon wire specimens under pure oxygen at one atmosphere of pressure for 25 hours at 1000°C,	
	(a) 0.584 mm diameter 1000X	30
	(b) 0.965 mm diameter 1000X	30
	(c) 1.575 mm diameter 1000X	31
5	Microstructure of NiO scale formed upon hole specimens under pure oxygen at one atmosphere of pressure for 25 hours at 1000°C,	
	(a) 1.575 mm diameter 1000X	32
	(b) 0.965 mm diameter 1000X	32
	(c) 0.584 mm diameter 1000X	33
6	Microstructure of NiO scale formed upon flat specimens under pure oxygen at one atmosphere of pressure for 25 hours,	
	(a) Specimens oxidized at 1000°C 1000X	34
	(b) Specimens oxidized at 800°C 1000X	34
7	Total scale thickness, X, versus oxidiation, t, for wire specimens,	
	(a) 0.584 mm diameter wire specimens	39
	(b) 0.965 mm diameter wire specimens	40
	(c) 1.575 mm diameter wire specimens	41

LIST OF FIGURES - Continued

Figure		Page
8	Total scale thickness, X versus oxidation time, t for hole specimens, (a) 1.575 mm diameter hole specimens	42
	(b) 0.965 mm diameter hole specimens	43
	(c) 0.584 mm diameter hole specimens	44
9	Average total scale thickness for the six oxidation times, $\overline{X}$, versus nickel surface curvature, 1/r	45
10	Mean grain intercept of the columnar layer $\overline{\lambda}_{COL}$, versus nickel surface curvature, 1/r, (a) Wire specimens	56
	(b) Hole specimens	56
11	Mean grain intercept of the equiaxed layer, $\overline{\lambda}_{EQ}$, versus nickel surface curvature, 1/r, (a) Wire specimens	58
	(b) Hole specimens	58
12	Equiaxed fraction of total scale thickness, X_{EQ}/X, versus nickel surface curvature, 1/r, (a) Specimens oxidized for 4 hours	59
	(b) Specimens oxidized for 9 hours	60
	(c) Specimens oxidized for 16 hours	61
	(d) Specimens oxidized for 25 hours	62
	(e) Specimens oxidized for 36 hours	63
	(f) Specimens oxidized for 49 hours	64
13	Columnarity of the outer layer, $\lambda_{COL}/\overline{\lambda}_{COL}$, versus nickel surface curvature, 1/r, (a) Specimens oxidized for 4 hours	69
	(b) Specimens oxidized for 9 hours	70
	(c) Specimens oxidized for 16 hours	71
	(d) Specimens oxidized for 25 hours	72
	(e) Specimens oxidized for 36 hours	73
	(f) Specimens oxidized for 49 hours	74
14	Total scale thickness, X, versus oxidiation time, t, extrapolated to t = 0 for wire and hole specimens, (a) 0.584 mm diameter wire specimens	78
	(b) 0.965 mm diameter wire specimens	78
	(c) 1.575 mm diameter wire specimens	79
	(d) 1.575 mm diameter hole specimens	80
	(e) 0.965 mm diameter hole specimens	80
	(f) 0.584 mm diameter hole specimens	81

LIST OF FIGURES - Continued

Figure		Page
15	Columnar layer thickness, X_{COL}, versus oxidation time, t, extrapolated to t = 0 for wire and hole specimens, (a) 0.584 mm diameter wire specimens	82
	(b) 0.965 mm diameter wire specimens	82
	(c) 1.575 mm diameter wire specimens	83
	(d) 1.575 mm diameter hole specimens	84
	(e) 0.965 mm diameter hole specimens	84
	(f) 0.584 mm diameter hole specimens	85
16	Total scale thickness, X, versus oxidation time, t, for flat spcimens, (a) Specimens oxidized at 1000°C	88
	(b) Specimens oxidized at 800°C	89
17	Equiaxed fraction of total scale thickness, X_{EQ}/X, versus oxidation time, t, for flat specimens	92
18	Total scale thickness, X, versus oxidation time, t, extrapolated to t = 0 for flat specimens, (a) Specimens oxidized at 1000°C	94
	(b) Specimens oxidized at 800°C	94
19	Columnar layer thickness, X_{COL}, versus oxidation time, t, extrapolated to t = 0 for flat specimens, (a) Specimens oxidized at 1000°C	95
	(b) Specimens oxidized at 800°C	95
20	Schematic representation of the proposed two-stage oxidation model	101
21	Scanning electron micrograph illustrating the surface morphology of NiO grown upon a flat Nickel 270 specimen at 800°C for 1 hour. Note the ridges of NiO along the oxide grain boundaries	102
22	Method of calculating the NiO grain boundary surface area per unit volume of scale, $S_{V\ TOTAL}$	109
23	NiO grain boundary surface area per unit volume of scale, $S_{V\ TOTAL}$, versus total scale thickness, X, for wire specimens	113

LIST OF FIGURES - Continued

Figure		Page
24	NiO grain boundary surface area per unit volume of scale, $S_{V\ TOTAL}$, versus total scale thickness, X, for hole specimens	115
25	Method of calculating the radius of the metal/oxide interface, $R_{M/O}$, (a) For wire specimens	118
	(b) For hole specimens	119
26	Total scale thickness, X, versus the radius of the metal/oxide interface, $R_{M/O}$, (a) 0.584 mm diameter wire specimens	123
	(b) 0.965 mm diameter wire specimens	124
	(c) 1.575 mm diameter wire specimens	125
	(d) 1.575 mm diameter hole specimens	126
	(e) 0.965 mm diameter hole specimens	127
	(f) 0.584 mm diameter hole specimens	128
27	Ratio of calculated to true volume of NiO formed, V_C/V_T, versus nickel surface curvature, 1/r, for 25 hours of oxidation	130
II-1	Method of determining the "calculated" total scale thickness, $X = R_O - R_I$, of NiO formed upon wire specimens	145
II-2	Method of determining the "calculated" total scale thickness, $X = R_O - R_I$, of NiO formed upon hole specimens	146

Abstract of Dissertation Presented to the Graduate Council of the University of Florida in Partial Fulfillment of the Requirements for the Degree of Doctor of Philosophy

THE ROLE OF NICKEL SURFACE CURVATURE IN THE HIGH-TEMPERATURE OXIDATION OF NICKEL 270

By

H. John Healey, Jr.

June 1978

Chairman: Dr. Frederick N. Rhines
Major Department: Materials Science and Engineering

High-temperature oxidation of Nickel 270 (nominally 99.99 + % nickel) results in the formation of a bi-layered NiO scale composed of an outer layer of columnar grains and an inner layer of equiaxed grains. Measurement of the total scale thickness formed at 1000°C on cylindrical surfaces of nickel (wires for convex surfaces, drilled holes for concave surfaces) has shown that scale thickness is proportional to the surface curvature (i.e. reciprocal of the cylindrical radius). Comparison of these measurements with those of the equiaxed layer thickness has revealed that the equiaxed layer becomes a linearly increasing fraction of the total scale thickness as nickel surface curvature decreases. This trend is associated with an increased plastic deformation of the NiO, owing to the influence of nickel surface curvature upon

the space into which the oxide is growing. Quantitative measurement of the grain size in both layers of the scale has confirmed that the mean grain intercept always increases in proportion to the scale thickness, and that the NiO grain size is larger upon hole specimens than upon wire specimens. The initial grain size, which is presumed to depend upon the nucleation of NiO on the original metal surface, was the same on all convex surfaces, but varied from one concave surface to another. This behavior suggests that nucleation is influenced by the accessibility of the oxidizing atmosphere to the oxidizing surface, convex surfaces being more easily accessible than concave surfaces. Based upon the results of this research, a two-stage model of the high-temperature oxidation of nickel is proposed. The duration of the initial stage and, consequently, the onset of the later stage are controlled by nickel surface curvature.

Lest it be argued that the effect of nickel surface curvature upon the oxidation rate is purely geometric, due to a decrease or increase in the metal/oxide interfacial area during oxidation of wire and hole specimens, respectively, it is pointed out that the volume of NiO scale formed is not proportional to the metal/oxide interfacial area.

CHAPTER I

INTRODUCTION

Several investigations [1-5] have shown an effect of surface curvature upon the oxidation rate of metals. Iida et al. [1] and Hancock and Fletcher [2] discovered that the particle size of nickel powder influenced its oxidation rate. More detailed experiments by Romanski [3, 4] and Borovski et al. [5] also demonstrated the existence of a surface curvature effect upon oxidation kinetics. Romanski concluded, by surveying the contour of iron specimens, that thinner or thicker layers of reaction products may form upon convex and concave surfaces, respectively [3], and that specimen size and shape influenced the oxidation kinetics of iron, nickel and copper [4]. Borovski et al. [5], by surveying the contour of nickel specimens, found the rate of NiO growth to diminish with sharpness of convexity.

While these experiments verified an effect of surface curvature upon the oxidation rate, they did not attribute this effect to any variable in the oxidation process as influenced by surface curvature. The current research offers results which indicate that nickel surface curvature affects the lateral, compressive stresses generated

during oxidation. In so doing, the plastic response of NiO to relieve these stresses is affected, which, in turn, affects the microstructural evolution and thickening of NiO.

1.1. The Scientific Background for the Research

The current research has required a background of knowledge in several areas of high-temperature oxidation. These areas include the microstructure of NiO and its effect upon scale thickening, the mechanical properties of NiO, the transport of reactants in NiO, the stresses developed within the scale during oxidation, the plastic deformation of NiO, and the nucleation and growth of NiO. Knowledge of each of these subjects becomes essential since this research concerns the microstructural evolution and thickening of NiO, and since it proposes a mechanism of high-temperature oxidation involving counter diffusion of reactants, generation of stresses within the scale and plastic deformation of the oxide.

1.1.1. The Microstructure of NiO

Little doubt exists among the investigators of nickel high-temperature oxidation that the NiO formed upon flat, nickel surfaces, under pure oxygen at one atmosphere of pressure, is bi-layered [6-22]. The outer layer of the scale is composed of columnar grains and the inner layer of equiaxed grains, as viewed in section normal to the

metal/oxide interface. Sartell and Li [6] and Ueno [7] report the outer layer to be somewhat thicker than the inner layer for flat, nickel specimens oxidized between 900°C and 1200°C. These observations have also been made during the course of the current research as illustrated by Figure 1.

The structure of the inner layer of the bi-layered NiO scale is dependent upon the metal purity. In the case of pure nickel the NiO grain size of the inner and outer layer is approximately the same. In less pure nickel the inner layer is so fine that the grain boundaries become indistinguishable. These two structures are illustrated for Nickel 270 and Nickel 200, respectively, by Rhines and Connell [18, 19].

Porosity has been reported by nearly every investigator of the structure of NiO scales. Pores at the metal/oxide interface have been attributed to impurities upon the metal surface by Païdassi and Berry [14]. A frequent cause of porosity within the scale, particularly at oxide grain boundaries, is the presence of carbon in the nickel. This is probably the origin of the intergranular porosity reported by Hales and Hill [23] and Evans et al. [24], which they ascribed to condensed nickel vacancies. Metallographic fall-out is clearly a cause for the formation of much of the irregular porosity that has been reported. Rhines and Wolf [16] suggested that such cavities were analogous to the pores that form in metals during

1000X

Figure 1. Microstructure of NiO scale formed upon a flat specimen under pure oxygen at one atmosphere of pressure for 49 hours at 1000°C.

high-temperature creep. Similar evidence is reported by Hussey et al. [25]. This is not to contend that blisters, spalls and a variety of discontinuities in the scale are unreal, but simply that they arise from causes that are unrelated to the basic mechanism of the oxidation of nickel.

1.1.2. The Effect of the Microstructure of NiO Upon the Oxidation Rate

A correlation between the microstructure of the scale and the oxidation rate was probably first noticed by Pfeil [26] in 1929 who, working with iron, associated oxide grain growth with oxide scale growth. Since then, grain growth in thin films of NiO has been observed by Phelps et al. [8] and Perrow et al. [27, 28], and in thick scales by Rhines and Connell [18, 19]. Graham et al. [29], working with nickel single crystals, found that the rate of growth of polycrystalline NiO was faster than that of monocrystalline NiO, and that a fine-grained oxide thickened faster than a coarse-grained oxide.

1.1.3. Mechanical Properties of NiO

Since oxidation kinetics are affected by the mechanical properties of the oxide it becomes important to investigate these properties for NiO. Two properties of NiO are nearly equal to those of nickel at 1000°C. Tylecote [30] reported the thermal expansion coefficient of NiO to be 17.1×10^{-6} while that of nickel was 17.6×10^{-6}, and Rhines and Wolf [16] found the creep rates of NiO and

nickel to be approximately the same. At elevated temperature, above 700°C, a number of investigators [10, 24, 31, 32] have found NiO to be ductile. These findings serve to explain the observation of Bruce and Hancock [33] that nickel produces an adherent, crack-free oxide scale at temperatures from 800°C to 1000°C. Another investigation by Bruce and Hancock [34] yielded values of Young's Modulus which decreased with increasing temperature. Specific values were: 800°C - 46 to 60 x 10^6 psi; 900°C - 30 x 10^6 psi; and 1000°C - 37 x 10^6 psi.

1.1.4. The Transport of Reactants in NiO

There have been several studies done on the diffusion of nickel through NiO. The results of diffusivity determinations are as follows:

$D_{Ni} = 4.4 \times 10^{-4} \exp(-44.2 \text{ kcal/RT})$ Shim and Moore [35]

$D_{Ni} = 1.83 \times 10^{-3} \exp(-45.6 \text{ kcal/RT})$ Choi and Moore [36]

$D_{Ni} = 1.7 \times 10^{-2} \exp(-56.0 \text{ kcal/RT})$ Linder and Akerstrom [37]

All experiments used both polycrystalline and monocrystalline NiO and the activation energies for nickel diffusion were the same. Therefore, nickel ions diffuse through the NiO lattice and not along oxide grain boundaries.

The diffusion of oxygen through NiO has been recognized by several investigators to play an important role in the oxidation of nickel [20, 21, 38]. O'Keefe and Moore [38] reported only a slight amount of oxygen diffusion

through monocrystallline NiO, $D_o = 1 \times 10^{-5}$ exp (-54 kcal/RT). Volpe and Reddy [39] found a large amount of oxygen diffusion through polycrystalline NiO, $D_o = 4.8 \times 10^{-1}$ exp (-10.8 kcal/RT). From these results, oxygen apparently diffuses through NiO along its grain boundaries at a rate approximately an order of magnitude faster than the diffusion of nickel through NiO grains.

Preferential diffusion of oxygen along oxide grain boundaries is not uncommon among oxides. It has been reported for Al_2O_3 by Kuise [40] and Oshi and Kingery [41], for Cu_2O by Wilkins and Rideal [42] and Moore et al. [43] and for MgO by Hashimoto and Hama [44]. Caplan and Sproule [45] stated that polycrystalline Cr_2O_3 grows by outward diffusion of chromium ions and inward diffusion of oxygen ions along Cr_2O_3 grain boundaries.

Marker movement studies have demonstrated the existence of counter diffusion of the reactants through an oxide scale. In his work with iron, Pfeil [26] noticed that inert matter, originally upon the metal surface, had been enveloped by the oxide scale during oxidation. Thus, new oxide must have formed above and beneath the inert markers. Counter diffusion of the reactants, in this case iron outward and oxygen inward, satisfactorily explains Pfeil's observation. Others have duplicated the work of Pfeil using nickel [6, 46, 47]. These experiments have always produced NiO scales with the markers

located between the outer, columnar layer and the inner, equiaxed layer of the scale.

1.1.5. Stresses Developed Within the Scale

The first direct evidence of stress within an oxide scale was found by U. R. Evans [48] in 1927 in his film stripping experiments with iron. Upon separation from its substrate, by anodic or chemical means, the iron oxide curled up. Since then, a number of experiments have been performed indicating the existence of stress within an NiO scale. Ueno [7] purposely formed a black/green bi-layered scale on one side of a nickel coupon and a black/black bi-layered scale on the other. This resulted in a curling of the specimen and, following electrochemical removal of each scale, only the black/green bi-layered scale exhibited bending. Thus, the stress was greatest in the inner, green layer of the scale and it was compressive due to the direction of bending. Dankov and Churaev [49] demonstrated the existence of stress within NiO through curling of thin nickel foil after oxidation on one side only. Other curling experiments [16, 50] showed that an initially curved specimen, oxidized simultaneously on both sides, continued to curl tighter in the original sense. Rhines and Wolf [16] found flat nickel foil specimens to increase in surface area after oxidation at 1000°C. An average, lateral stress within the scale of approximately 1500 psi was calculated from the mean

values of lateral extension and creep and oxidation data for nickel. A similar increase in surface area of thin, nickel foil was also observed by Denisenko and Skorokhod [51] and Noris [52].

Similar effects have been observed in the high-temperature oxidation of many metals. The increase in surface area during oxidation was seen by Cathcart et al. [53] for uranium. Other metals showing the effects of stress within the oxide scale have been copper [54, 55], tantalum [56] and niobium [57].

1.1.6. Plastic Deformation of NiO

Evidence for plastic deformation of NiO scales appears throughout the literature. Hales [58] noted the presence of dislocations in the outer, columnar layer resembling those found in metal creep specimens. Cathcart et al. [59] found a mosaic structure, also in the outer, columnar layer, indicating a sub-grain network. A similar observation was made by Phelps et al. [8] who associated the sub-grain network with recovery from a plastically strained state. Vernon and Spooner [32] suggested that deformation of NiO occurred during oxidation based on their observation of slip lines on the crystals of the scale. Creep of NiO at elevated temperature has been measured by Antill and Washburn [60], Menzie and Aldred [13] and Rhines and Wolf [16]. Rhines and Connell [19] stated that when the nickel substrate is thin enough the stress developed within the

oxide is sufficient to cause bending or elongation by creep, but when the nickel substrate is too massive the plastic response to the stress is extrusion of oxide outward along NiO grain boundaries. This latter phenomenon has been seen, by scanning electron microscopy, to produce ridges of NiO outlining the NiO grain boundaries at the external surface of the scale [18]. As growth of the NiO scale proceeds, these ridges become lower and broader and the external surface takes on a cusped appearance. With further oxidation the external surface becomes faceted.

Most oxides, being sufficiently plastic at high temperature, have exhibited deformation during oxidation. This has been found true for iron by Maldy [61] and for uranium by Cathcart et al. [53]. Caplan and Sproule [45] proposed an oxidation mechanism for chromium involving the generation of compressive stresses within Cr_2O_3 followed by plastic deformation and wrinkling of the oxide.

1.1.7. Nucleation of NiO and Growth of Thin Films

Robin [62], Martins [63], Lozinsky and Antipova [64] and Wood and Chattopadhyay [65] found that the first nuclei of NiO to form did so along grain boundaries of the metal. Later nucleation probably involves the formation of many NiO nuclei upon each nickel grain since the grain size of NiO has been reported to be much finer than that of the underlying nickel [14, 22]. Holloway and Hudson [66] determined that, prior to complete coverage of the metal,

the oxide existed as small islands only a few atoms thick and growing by the addition of oxygen ions at their edges. Presumably, this edgewise growth continues until the islands of NiO impinge, one upon the other.

Cold work and surface preparation can affect the nucleation of NiO. Gulbransen [67] detected the appearance of many oxide nuclei on each metal grain reflecting the presence of defects and inclusions. He also found the density of oxide growth centers to be of the same order of magnitude as the density of dislocations. Caplan et al. [68] demonstrated that cold work influenced both the grain size and growth rate of NiO, and that cold work masked any effect of epitaxi, thus yielding a uniformly thick oxide unrelated to the underlying nickel structure. That there is an effect of surface preparation upon oxidation has been shown by several investigators [12, 69-71]. According to Wood and Wright [12], the oxidation rate appears to be partially determined by specimen history, probably because it establishes the topography and nature of the surface exposed to the oxidizing atmosphere.

Epitaxial relationships between oxide and metal were seen by Newkirk and Martin [72] and Caplan et al. [68] with the (111) plane of the oxide parallel to the (111) plane of the metal, and by Papageorgopoulous and Chen [73] with the (100) plane of the oxide parallel to the (100) plane of the metal. This epitaxial effect could contribute

to the change in oxide growth rate with orientation of the underlying nickel as found by Anderson and Ritchie [74], Carlsen [75], Graham et al. [76] and Herchl et al. [22]. Mostly, however, the orientation of the oxide is random with respect to the metal [72].

Research into thin film (less than 30 Å) growth has yielded two rate laws. An exponential rate was deduced by Tammann [77] in 1920 and corroborated later by others [78-85]. More recently, a few studies [86-89] have obtained a logarithmic rate.

1.1.8. Parabolic Growth of NiO, The Classical Model

The concept of parabolic growth of NiO, i.e., thickness proportional to time$^{1/2}$, was first put forward by Pilling and Bedworth [90] in 1923 and substantiated later by others [69, 91-97]. Wagner [98], claiming the inward diffusion of oxygen suggested by Pilling and Bedworth was insignificant, proposed the outward diffusion of nickel ions through the scale to the external surface. There oxygen ions were met, resulting in the formation of new NiO. Douglass [99], also claiming that oxygen diffusion was negligible, referred to the parabolic rate law as being the only one having any real significance in the sense that rates can be predicted from a knowledge of fundamental parameters. Subsequent research has revealed that the parabolic growth model fails to explain four important points: (1) the polycrystalline oxide scale thickens at a rate that is

an order of magnitude greater than predicted by the diffusion of nickel alone [18]; (2) the rate of oxidation diminishes more rapidly than parabolic behavior suggests [18]; (3) the oxide scale envelops inert particles [26]; and (4) the growing scale develops compressive stresses during oxidation [16].

1.1.9. Non-Parabolic Growth of NiO

Many investigators [8, 18, 19, 87, 100-103] have detected non-parabolic growth of NiO. Rhines and Connell [18] have proposed an alternative mechanism of oxidation to that suggested by Wagner [98] which accounts for the deficiencies in the parabolic growth model. They have suggested that the diffusion process involves two ionic species--nickel diffusing outward through the NiO lattice and oxygen diffusing inward along NiO grain boundaries. The two meet at the NiO grain boundaries whereupon new oxide forms, creating a lateral "wedging effect" upon neighboring grains. Because of the attachment of NiO to the nickel substrate, a lateral, compressive stress is generated within the scale. Plastic deformation of NiO relieves these compressive stresses. The passage of shear across NiO grain boundaries increases the local grain boundary curvature [104] and, in response, the grain boundaries migrate under the forces of surface tension. An increase in the local grain boundary curvature must occur for grain boundaries to migrate because pinning

forces at the metal/oxide interface and the external surface must be overcome. As the grain boundaries sweep throughout the scale, they distribute new oxide throughout the scale volume by providing a moving reaction front. The end result of this model of high-temperature nickel oxidation is NiO grain growth occurring concurrently with NiO scale growth [18, 19].

1.1.10 Summary of Established Facts Concerning the High-Temperature Oxidation of Nickel

The foregoing literature survey has established the following facts about the high-temperature oxidation of nickel:

1) The NiO scale produced at elevated temperature is bi-layered and is composed of an outer layer of columnar grains and an inner layer of equiaxed grains.
2) The microstructure of NiO influnces the oxidation rate. Polycrystalline NiO grows faster than monocrystalline NiO and a fine-grained oxide grows faster than a coarse-grained oxide.
3) NiO grain growth accompanies NiO scale growth.
4) The creep rates and thermal expansion coefficients of NiO at 1000°C are nearly equal to those of nickel at 1000°C making for an adherent, crack-free oxide scale.
5) Nickel ions diffuse through the NiO lattice, not along NiO grain boundaries.

6) Oxygen ions diffuse along NiO grain boundaries at a rate approximately an order of magnitude faster than the diffusion of nickel ions through the NiO lattice.

7) Inert matter, originally upon the metal surface, is always found near the columnar/equiaxed interface after oxidation.

8) Lateral, compressive stresses are generated within the scale during oxidation.

9) Plastic deformation of NiO occurs during oxidation.

10) Ridges of NiO, located at the external surface of the scale upon columnar grain boundaries, appear early in oxidation. As oxidation proceeds the external surface develops a cusped appearance and, eventually, becomes faceted.

11) Nucleation of the first oxide occurs along grain boundaries of the metal. Many NiO nuclei form upon a single nickel grain and begin to grow by the addition of oxygen ions at their edges.

12) Cold work and surface preparation can affect the nucleation of NiO, thereby affecting the oxidation rate.

13) Epitaxial growth of NiO occurs, but mostly the grain size of the oxide is very much finer than that of the underlying nickel and shows little indication of being related in orientation to the metal.

14) Growth of thin films of NiO is disputed. Some investigators have determined an exponential rate while others have found a logarithmic rate.

15) Growth of NiO (greater than 30 Å) is characterized by a rate equation having a time exponent of 0.50 (parabolic) or less (non-parabolic).

These facts concerning the high-temperature oxidation of nickel have been recognized by the current research in designing the experiment or in interpreting the results.

1.2. The Objective of the Research

Little quantitative research has been undertaken to study the microstructural evolution of NiO which occurs concurrently with scale thickening. The investigations which have been undertaken [18, 19] utilized flat nickel specimens and showed that NiO grain growth occurred simultaneously with NiO scale growth. Generation of lateral, compressive stresses during oxidation, causing plastic deformation of the oxide, was determined to be a very important feature of the oxidation process. The current research was designed to discover the interrelations among NiO scale growth, NiO microstructure, stress generation within the scale and plastic deformation of the oxide. Variation of nickel surface curvature was thought to provide a means by which to study these interrelations,

thus improving the current understanding of the high-temperature oxidation of nickel.

CHAPTER II

EXPERIMENTAL TECHNIQUES

Some of the experimental procedures used in this research had been developed during the course of a previous research.* These procedures, as well as those newly developed, are described in the following paragraphs.

2.1. Specimen Preparation

To evaluate the effect of nickel surface curvature upon the microstructural evolution and thickening of NiO, two types of Nickel 270 (nominally 99.99 + % nickel) specimens were oxidized. To provide a range of surface curvature from positive (convex) to negative (concave), the external surfaces of wires, having diameters of 1.575 mm, 0.965 mm and 0.584 mm, and the internal surfaces of holes (hole specimens), having corresponding diameters, were oxidized. Nickel 270 wire specimens were prepared by drawing 1.575 mm wire through successive dies yielding the two smaller

*"Control of Environmental Surface Reactions," Final Report, June 15, 1972 to September 15, 1973, F. N. Rhines, E. D. Verink, Jr., L. L. Hench and Associates, Department of Materials Science and Engineering, University of Florida. Prepared for NSF under Grant No. GH-34550.

diameters to be used. Hole specimens were drilled in 3.175 mm thick flat discs machined from one inch rods. Each hole was drilled at a distance of 7.950 mm from a 1.575 mm diameter central hole and at a distance of 5.791 mm from each other. Enough wire and hole specimens were made to insure that either three wires or three holes of each diameter were simultaneously oxidized.

To evaluate the effect of oxidiation temperature upon the microstructural evolution and thickening of NiO, flat Nickel 270 specimens were oxidized at 1000°C and 800°C. These specimens were cut into 1.66 mm x 12.7 mm x 12.7 mm coupons from 1.6 mm thick Nickel 270 sheet.

Just prior to the oxidizing treatment, each specimen was cleaned according to the method outlined in Table I. Following cleaning, oxidation was initiated within one hour.

2.2. Oxidation

The oxidation treatments for Nickel 270 wire, hole and flat specimens were conducted in an all-metal system consisting of stainless steel (AISI Type 316) gas trains, a Nickel 200 (nominally 99.40 % nickel) thermocouple sheath, Nickel 270 specimen hangers and a Nickel 200 closed reaction tube. As such, Figure 2, the only metal exposed to the high-temperature oxidizing environment was nickel. Heat was applied to the reaction tube by a resistance-heated, split-tube furnace which could be brought

Table I

Standardized Surface Preparation for Nickel 270 Specimens

1. Grind with 600 grit SiC abrasive when shape of specimen permits.

2. Clean with the following agents in succession:

   (a) Acetone, 5 minutes, ultrasonic

   (b) Boiling H_2O (distilled), 5 minutes

   (c) Ethanol, 5 minutes, ultrasonic

   (d) H_2O (distilled), 5 minutes, ultrasonic

   (e) Ethanol, 5 minutes, ultrasonic

   (f) Air dry

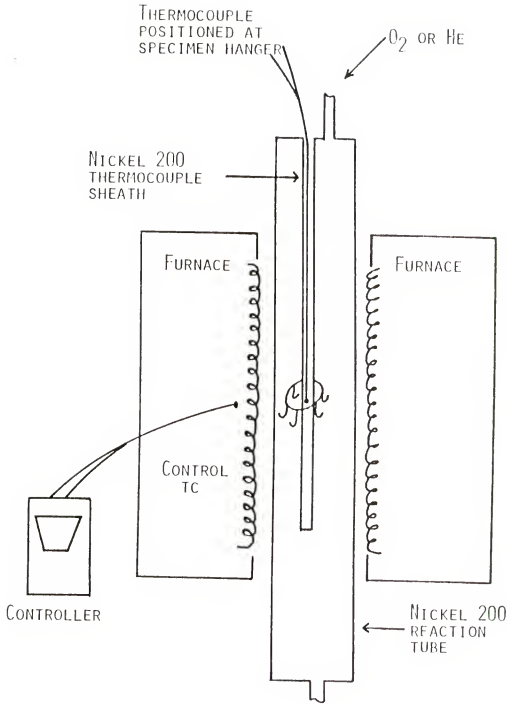

Figure 2. Schematic diagram of the oxidation system used for oxidizing the Nickel 270 specimens.

to temperature prior to placing it around the reaction tube. The temperature of this furnace was controlled by a chromel-alumel thermocouple connected to a Leeds-Northrup Electromax DAT on-off controller. Another chromel-alumel thermocouple was positioned inside the reaction tube to insure that the proper oxidation temperature was being maintained within ±5°C. A circulating water coolant at both ends of the reaction tube provided for a hot zone of approximately 50.8 mm.

The oxidation schedule began by flushing the cold reaction tube with high purity helium (AIRCO GRADE 5) for 15 minutes. Then, after placing the split-tube furnace around the nickel reaction tube, the wire, hole or flat specimens were heated to 1000°C (or 800°C for some flat specimens) while still maintaining the helium atmosphere. Upon reaching 1000°C (or 800°C), the specimens were given a 20 minute annealing treatment prior to oxidation. After annealing, the helium supply was turned off and high purity oxygen (AIRCO GRADE 5) was admitted to the reaction tube at about one atmosphere of pressure. This oxygen atmosphere was maintained for the entire oxidation period (4, 9, 16, 25, 36 or 49 hours). Following oxidation, the furnace was removed and the reaction tube was allowed to cool under oxygen to 400°C, whereupon the system was exposed to air.

The above oxidation schedule was carried out for six wire specimens or six hole specimens of each diameter for

each of the six oxidation times mentioned (three specimens of each diameter at a time). One flat specimen was oxidized for each of the six oxidation times at either 1000°C or 800°C.

2.3. Metallographic Preparation

The oxidized wire, hole and flat specimens were mounted so that the NiO surface to be examined was at 90° to the wire or hole axis, or at 90° to the plane of the Nickel 270 sheet. Table II outlines the methods that were used to produce high quality polished and etched surfaces.

2.4. Scale Thickness Measurements

All scale thickness measurements were made on a Bausch and Lomb Research II metallograph using a reticle scale calibrated against a stage micrometer at 1000X. Total scale thickness, X, and equiaxed layer thickness, X_{EQ}, measurements were recorded at a minimum of 15 positions on the NiO formed upon each wire or hole specimen, and 25 positions on that formed upon each flat specimen. In each case, the columnar layer thickness, X_{COL}, was obtained by taking the difference between total scale thickness and equiaxed layer thickness. Specimens which developed a non-uniform scale thickness were measured at

Table II

Metallographic Procedures

Mounting: Buehler plastimet

Mounting temperature: 150°C

Mounting pressure: 3000 psi

Mounting time: 7 minutes

Cool-down time: 5 minutes

Dimensions of mount: 1 1/4" diameter x 1" high

Electrical contact by screw into side of mount

Grinding: Automatic with 6 specimens simultaneously

120 grit SiC with water, 15 minutes

180 grit SiC with water, 15 minutes

320 grit SiC with water, 10 minutes

600 grit SiC with water, 10 minutes

Polishing: Automatic with 6 specimens simultaneously

6μ diamond, AB Texmet cloth, 4 hours

1μ (heavy) diamond, AB Texmet cloth, 4 hours

Table II - Continued

Electrolytic etching to develop microstructure of NiO:

Solution: 1 vol. HF (48%)
1 vol. CH_3 COOH (glacial)
4 vol. H_2O (distilled)

Anode: Specimen

Potential: 10 to 15 volts (open circuit)

Time: 20 to 40 seconds for wire or flat specimens
4 to 8 minutes for hole specimens

Temperature: 25°C

more positions than those which developed a relatively uniform scale thickness. Because six wire specimens or six hole specimens of each diameter were oxidized for each of the six oxidation times (4, 9, 16, 25, 36 or 49 hours), a total of 90 or more scale thickness measurements (either X, X_{EQ} or X_{COL}) were recorded for each condition of oxidation. With one flat specimen having been oxidized for each of the six oxidation times at either 1000°C or 800°C, a total of 25 or more scale thickness measurements (either X, X_{EQ} or X_{COL}) were taken for each condition of oxidation. A 95% confidence interval for the mean of X, X_{EQ} or X_{COL} was computed for the NiO formed upon all specimen geometries (1.575 mm, 0.965 mm and 0.584 mm diameter wire and hole specimens, and flat specimens oxidized at 1000°C and 800°C).

The ratio of the mean, equiaxed layer thickness to the mean, total scale thickness was determined for all specimen geometries in order to evaluate the effect of nickel surface curvature and oxidation temperature upon the microstructure of NiO.

2.5. Determination of Mean Grain Intercept

The number of NiO grain boundary intercepts made with a test line of known length was determined at positions within the oxide scale corresponding to Figure 3. These measurements were also carried out on a Bausch and Lomb Research II metallograph using a pre-calibrated test line of 0.074 mm in length at 1000X.

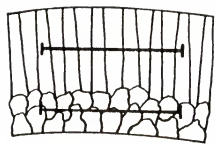

(a)

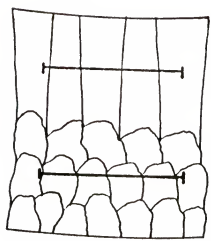

(b)

Figure 3. Test line orientation for determining the number of NiO grain boundary intercepts in the columnar and equiaxed layers, (a) NiO formed upon wire specimens, (b) NiO formed upon hole specimens.

Two values of the number of NiO grain boundary intercepts were determined for each of the wire and hole specimens: a columnar, $N_{L\ COL}$; and an equiaxed, $N_{L\ EQ}$. The columnar readings were taken at a position roughly halfway between the external surface and the columnar/equiaxed interface, and the equiaxed readings were taken roughly halfway between the columnar/equiaxed interface and the metal/oxide interface. Enough areas of the scale were measured on each specimen so that 400 or more NiO grain boundary intercepts were counted. Because six specimens of each wire or hole diameter were oxidized for each oxidation time, a total of 2400 or more NiO grain boundary intercepts were counted for each condition of oxidation. The mean values of the number of NiO grain boundary intercepts, along with their corresponding 95% confidence intervals, were computed and divided by the calibrated length of test line (0.074 mm) yielding corresponding values of N_L.

Mean grain intercept values, $\bar{\lambda}_{COL}$ or $\bar{\lambda}_{EQ}$, were obtained by taking the reciprocal of the corresponding N_L values. The ratio of the mean columnar layer thickness, as determined in section 2.4., to the mean grain intercept of the columnar layer was determined as a further evaluation of the effect of nickel surface curvature upon the microstructure of NiO.

CHAPTER III

EXPERIMENTAL RESULTS

Representative NiO scales formed upon wire, hole and flat Nickel 270 specimens are shown in Figures 4-6. The bi-layered nature of NiO produced at 1000°C for wire and hole specimens, and at 1000°C and 800°C for flat specimens is readily apparent. All scales were formed under pure oxygen at one atmosphere of pressure.

3.1. Growth of NiO Upon Curved Specimens

From Figures 4 and 5 it can be seen that nickel surface curvature influences both the total scale thickness and microstructure of NiO. These photomicrographs show the total scale thickness to increase with decreasing nickel surface curvature (increasing wire diameter and decreasing hole diameter), the NiO grain size to become finer upon wire specimens than upon hole specimens and the equiaxed layer thickness to become an increasing fraction of total scale thickness with decreasing nickel surface curvature.

3.1.1. Total Scale Thickness of NiO Formed Upon Wire and Hole Specimens

Total scale thickness measurements made on the NiO formed upon wire and hole specimens are presented in

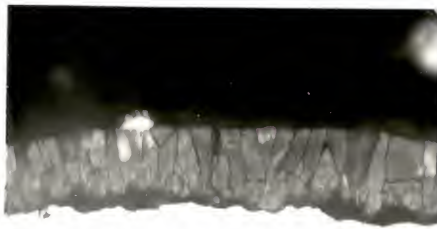

(a) 0.584 mm diameter. 1000X

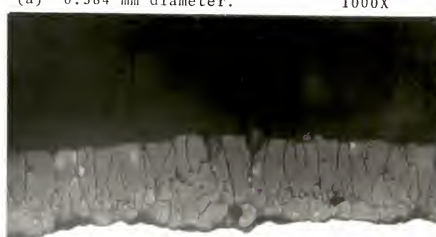

(b) 0.965 mm diameter. 1000X

Figure 4. Microstructure of NiO scale formed wire specimens under pure oxygen at one atmosphere of pressure for 25 hours at 1000°C.

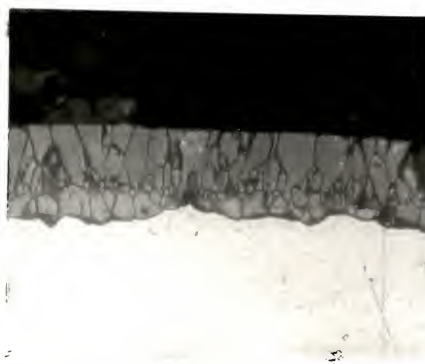

(c) 1.575 mm diameter. 1000X

Figure 4. (continued).

(a) 1.575 mm diameter. 1000X

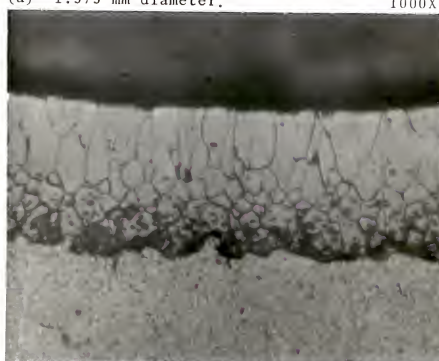

(b) 0.965 mm diameter. 1000X

Figure 5. Microstructure of NiO scale formed upon hole specimens under pure oxygen at one atmopshere of pressure for 25 hours at 1000°C.

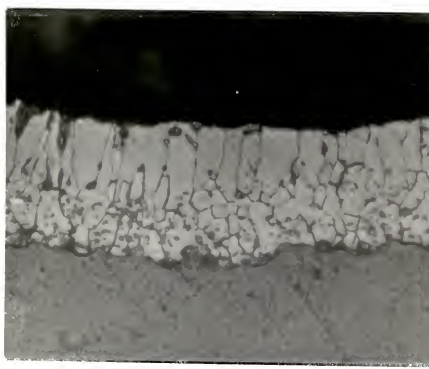

(c) 0.584 mm diameter. 1000X

Figure 5. (continued).

(a) Specimens oxidized at 1000°C. 1000X

(b) Specimens oxidized at 800°C. 1000X

Figure 6. Microstructure of NiO scale formed upon flat specimens under pure oxygen at one atmosphere of pressure for 25 hours.

Table III along with their corresponding 95% confidence intervals. These data, when plotted versus oxidation time, result in the experimental curves of Figures 7 and 8 for wire and hole specimens, respectively. The kinetic equations for these best-fit curves and their corresponding correlation coefficients are given. The curves labeled "calculated" in the figures represent the total thickness of NiO which should form upon the particular specimen based on geometric considerations and assuming flat specimen kinetics are operating at the 1000°C oxidation temperature (see Appendix II). The departure between experimental and calculated curves, in all cases, indicates the effect of nickel surface curvature upon scale thickening is not purely a geometric one. For all wire specimens the calculated curve lies above the experimental, while for all hole specimens the calculated curve lies below the experimental. The trend is one of ascending order from the smallest diameter wire to the smallest diameter hole.

When the average, total scale thickness for the six oxidation times, calculated from the data of Table III, is plotted against nickel surface curvature, Figure 9, two linear relationships are found--one for wire specimens and one for hole specimens. In each case, the average, total scale thickness for the six oxidation times increases linearly with decreasing nickel surface curvature, but the linear relationship found for hole specimens is displaced above that found for wire specimens.

Table III

Total NiO Scale Thickness Measurements for Wire and Hole Nickel 270 Specimens

Specimen Diameter (mm)	Surface Curvature, $1/r$ (mm^{-1})	Oxidation Time (hours)	Total Scale Thickness, X ($\times 10^{-3}$ mm)
0.584 wire	3.42	4	8.33 ± 0.20
0.965 wire	2.07	4	9.00 ± 0.21
1.575 wire	1.27	4	10.07 ± 0.33
1.575 hole	-1.27	4	16.53 ± 0.42
0.965 hole	-2.07	4	17.08 ± 0.47
0.584 hole	-3.42	4	16.32 ± 0.32
0.584 wire	3.42	9	13.09 ± 0.47
0.965 wire	2.07	9	14.05 ± 0.50
1.575 wire	1.27	9	14.69 ± 0.53
1.575 hole	-1.27	9	20.39 ± 0.56
0.965 hole	-2.07	9	19.79 ± 0.50
0.584 hole	-3.42	9	18.68 ± 0.39

Table III - Continued

Specimen Diameter (mm)	Surface Curvature, 1/r (mm^{-1})	Oxidation Time (hours)	Total Scale Thickness, X ($\times 10^{-3}$ mm)
0.584 wire	3.42	16	17.75 ± 0.36
0.965 wire	2.07	16	18.71 ± 0.36
1.575 wire	1.27	16	18.94 ± 0.41
1.575 hole	-1.27	16	29.08 ± 0.83
0.965 hole	-2.07	16	27.42 ± 0.78
0.584 hole	-3.42	16	29.78 ± 0.87
0.584 wire	3.42	25	19.05 ± 0.40
0.965 wire	2.07	25	21.06 ± 0.49
1.575 wire	1.27	25	23.57 ± 0.76
1.575 hole	-1.27	25	30.61 ± 0.94
0.965 hole	-2.07	25	33.53 ± 0.82
0.584 hole	-3.42	25	34.75 ± 0.76

Table III - Continued

Specimen Diameter (mm)	Surface Curvature, $1/r$ (mm^{-1})	Oxidation Time (hours)	Total Scale Thickness, X ($\times 10^{-3}$ mm)
0.584 wire	3.42	36	22.58 ± 0.53
0.965 wire	2.07	36	23.90 ± 0.45
1.575 wire	1.27	36	27.01 ± 0.68
1.575 hole	-1.27	36	38.81 ± 0.68
0.965 hole	-2.07	36	41.03 ± 1.07
0.584 hole	-3.42	36	42.02 ± 0.43
0.584 wire	3.42	49	26.90 ± 0.49
0.965 wire	2.07	49	28.56 ± 0.41
1.575 wire	1.27	49	30.76 ± 0.62
1.575 hole	-1.27	49	40.99 ± 1.38
0.965 hole	-2.07	49	42.77 ± 1.18
0.584 hole	-3.42	49	44.66 ± 1.19

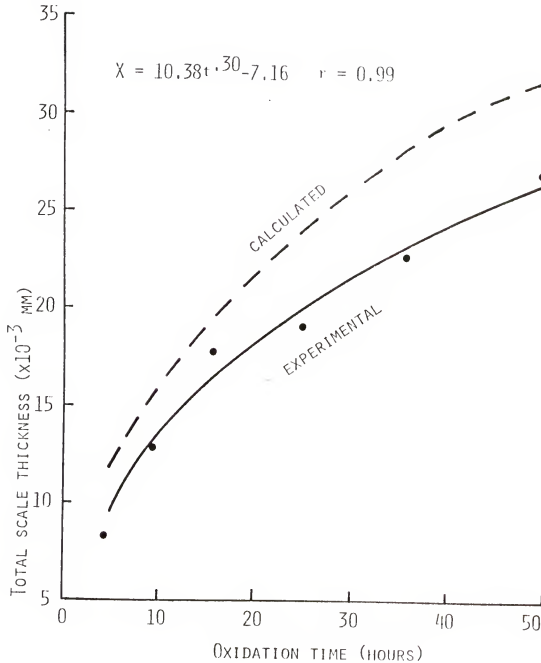

Figure 7. Total scale thickness, X, versus oxidation, t, for wire specimens.

(a) 0.584 diameter wire specimens.

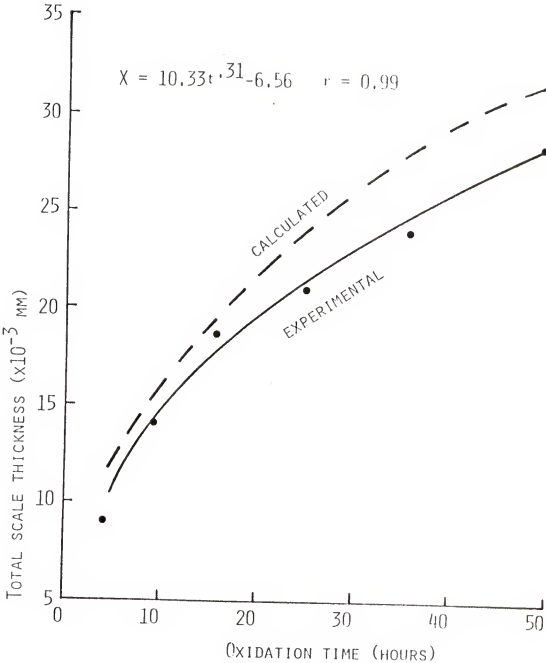

Figure 7. (continued).

(b) 0.965 mm diameter wire specimens.

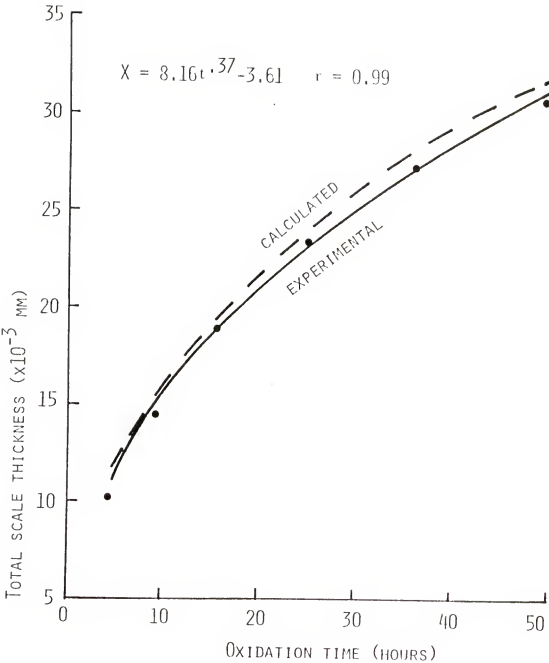

Figure 7. (continued).

(c) 1.575 mm diameter wire specimens.

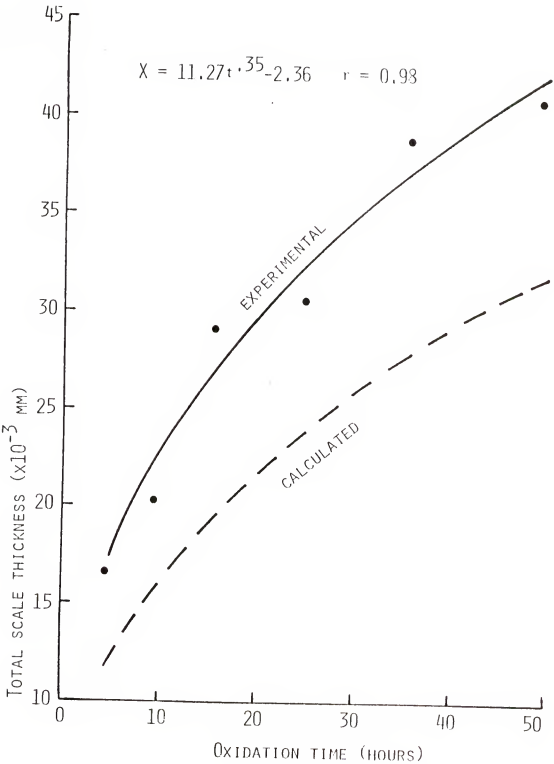

Figure 8. Total scale thickness, X, versus oxidation time, t, for hole specimens.

(a) 1.575 mm diameter hole specimens.

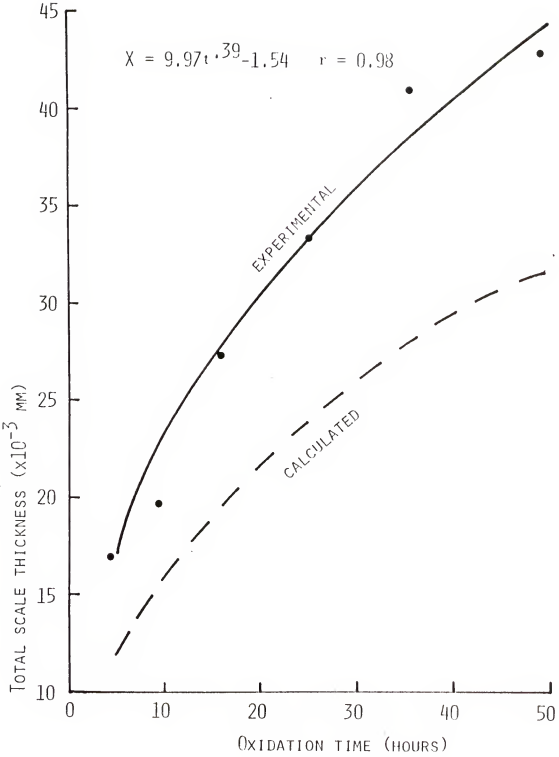

Figure 8. (continued).

(b) 0.965 mm diameter hole specimens.

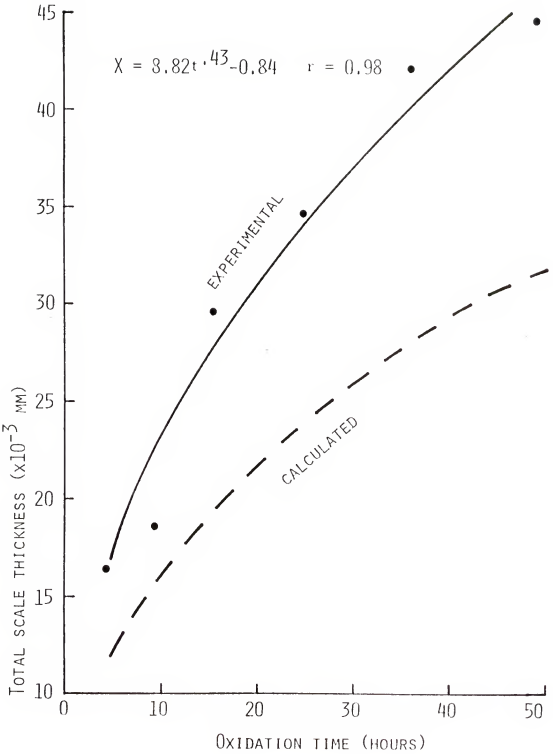

Figure 8. (continued).

(c) 0.584 mm diameter hole specimens.

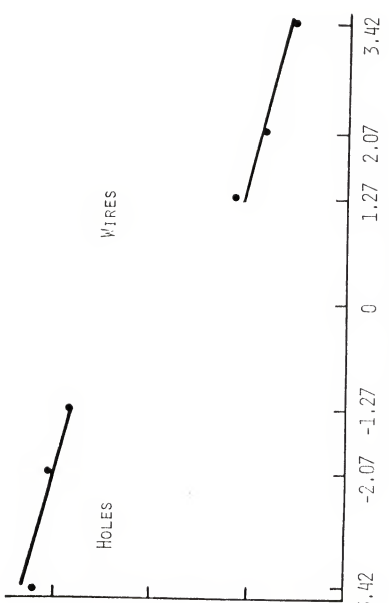

Figure 9. Average total scale thickness for the six oxidation times, $\bar{X}$, versus nickel surface curvature, 1/r.

3.1.2. Microstructure of NiO Formed Upon Wire and Hole Specimens

Referring to Figures 4 and 5, there are two immediately distinguishable effects of nickel surface curvature upon NiO microstructure. The NiO grain size is larger for the oxide formed on the internal surfaces of holes and the fraction of total scale thickness composed of equiaxed grains increases with decreasing nickel surface curvature. These observations are confirmed by the results of mean grain intercept determinations and the relative thickness of scale layers. Mean values of the number of NiO grain boundary intercepts for the columnar and equiaxed layers, along with corresponding 95% confidence intervals, are recorded in Table IV. These results have been converted into mean grain intercept values for the columnar and equiaxed layers, $\lambda = 1/N_L$,* and are shown in Table V. The relative thickness of scale layers, X_{EQ}/X, is given in Table VI.

Graphs of mean grain intercept values for the outer, columnar grains versus nickel surface curvature are shown in Figure 10. After a given oxidation time, the $\bar{\lambda}_{COL}$ for any hole specimen is larger than the $\bar{\lambda}_{COL}$ for any wire specimen. These graphs also demonstrate that as the wire surface curvature decreases, the mean grain intercept of

---

*N_L is the mean value of the number of NiO grain boundary intercepts, for either the columnar or equiaxed layer, divided by the length of test line (0.074 mm) and $\bar{\lambda}$ is the corresponding mean grain intercept.

Table IV

Mean Values of the Number of NiO Grain Boundary Intercepts for the Columnar and Equiaxed Layers of the Scale Formed Upon Wire and Hole Nickel 270 Specimens

Specimen Diameter (mm)	Surface Curvature, 1/r (mm^{-1})	Oxidation Time (hours)	Mean Value of the Number of NiO Grain Boundary Intercepts for the Columnar Layer	Mean Value of the Number of NiO Grain Boundary Intercepts for the Equiaxed Layer
0.584 wire	3.42	4	42.00 ± 1.38	45.52 ± 1.67
0.965 wire	2.07	4	38.54 ± 1.65	43.53 ± 2.10
1.575 wire	1.27	4	36.76 ± 2.40	41.34 ± 2.36
1.575 hole	-1.27	4	17.50 ± 1.47	23.87 ± 0.63
0.965 hole	-2.07	4	19.60 ± 0.89	27.01 ± 0.85
0.584 hole	-3.42	4	20.02 ± 1.17	29.84 ± 0.79
0.584 wire	3.42	9	36.72 ± 1.21	39.18 ± 1.62
0.965 wire	2.07	9	32.40 ± 0.87	32.56 ± 1.30
1.575 wire	1.27	9	28.68 ± 1.00	28.14 ± 1.36
1.575 hole	-1.27	9	19.08 ± 0.94	21.39 ± 0.72
0.965 hole	-2.07	9	19.53 ± 0.91	23.34 ± 0.70
0.584 hole	-3.42	9	22.90 ± 0.82	26.65 ± 0.88

Table IV - Continued

Specimen Diameter (mm)	Surface Curvature, 1/r (mm^{-1})	Oxidation Time (hours)	Mean Value of the Number of NiO Grain Boundary Intercepts for the Columnar Layer	Mean Value of the Number of NiO Grain Boundary Intercepts for the Equiaxed Layer
0.584 wire	3.42	16	25.92 ± 1.00	28.50 ± 1.38
0.965 wire	2.07	16	23.02 ± 0.93	24.88 ± 1.05
1.575 wire	1.27	16	20.00 ± 0.64	19.14 ± 1.14
1.575 hole	-1.27	16	13.57 ± 0.51	18.27 ± 0.91
0.965 hole	-2.07	16	13.60 ± 0.56	20.50 ± 1.10
0.584 hole	-3.42	16	14.52 ± 0.78	22.26 ± 0.65
0.584 wire	3.42	25	24.50 ± 0.93	25.70 ± 1.68
0.965 wire	2.07	25	22.46 ± 0.77	25.28 ± 1.11
1.575 wire	1.27	25	18.56 ± 0.64	19.42 ± 1.28
1.575 hole	-1.27	25	11.56 ± 0.69	16.08 ± 0.59
0.965 hole	-2.07	25	12.21 ± 0.73	17.88 ± 0.70
0.584 hole	-3.42	25	11.97 ± 0.73	18.82 ± 0.84

Table IV - Continued

Specimen Diameter (mm)	Surface Curvature, 1/r (mm^{-1})	Oxidation Time (hours)	Mean Value of the Number of NiO Grain Boundary Intercepts for the Columnar Layer	Mean Value of the Number of NiO Grain Boundary Intercepts for the Equiaxed Layer
0.584 wire	3.42	36	18.62 ± 0.74	19.76 ± 1.30
0.965 wire	2.07	36	17.76 ± 0.62	19.68 ± 0.91
1.575 wire	1.27	36	15.78 ± 0.55	15.46 ± 0.62
1.575 hole	-1.27	36	9.91 ± 0.39	12.90 ± 0.52
0.965 hole	-2.07	36	10.51 ± 0.43	14.94 ± 0.62
0.584 hole	-3.42	36	10.56 ± 0.38	15.06 ± 0.56
0.584 wire	3.42	49	19.36 ± 0.70	21.64 ± 1.25
0.965 wire	2.07	49	17.76 ± 0.52	18.16 ± 1.01
1.575 wire	1.27	49	14.80 ± 0.56	15.50 ± 1.01
1.575 hole	-1.27	49	8.99 ± 0.45	11.51 ± 0.31
0.965 hole	-2.07	49	9.03 ± 0.46	12.87 ± 0.51
0.584 hole	-3.42	49	9.14 ± 0.60	12.94 ± 0.51

Table V

Mean Grain Intercept Values for the Columnar and Equiaxed Layers of the Scale Formed Upon Wire and Hole Nickel 270 Specimens

Specimen Diameter (mm)	Surface Curvature, 1/r (mm^{-1})	Oxidation Time (hours)	Mean Grain Intercept for the Columnar Layer, $\bar{\lambda}_{COL}$ ($\times 10^{-3}$ mm)	Mean Grain Intercept for the Equiaxed Layer, $\bar{\lambda}_{EQ}$ ($\times 10^{-3}$ mm)
0.584 wire	3.42	4	1.76	1.62
0.965 wire	2.07	4	1.92	1.70
1.575 wire	1.27	4	2.01	1.79
1.575 hole	-1.27	4	4.23	3.10
0.965 hole	-2.07	4	3.78	2.74
0.584 hole	-3.42	4	3.70	2.48
0.584 wire	3.42	9	2.02	1.89
0.965 wire	2.07	9	2.28	2.27
1.575 wire	1.27	9	2.58	2.63
1.575 hole	-1.27	9	3.88	3.46
0.965 hole	-2.07	9	3.79	3.17
0.584 hole	-3.42	9	3.23	2.78

Table V - Continued

Specimen Diameter (mm)	Surface Curvature, 1/r (mm^{-1})	Oxidation Time (hours)	Mean Grain Intercept for the Columnar Layer, $\bar{\lambda}_{COL}$ ($\times 10^{-3}$ mm)	Mean Grain Intercept for the Equiaxed Layer, $\bar{\lambda}_{EQ}$ ($\times 10^{-3}$ mm)
0.584 wire	3.42	16	2.85	2.60
0.965 wire	2.07	16	3.21	2.97
1.575 wire	1.27	16	3.70	3.87
1.575 hole	-1.27	16	5.45	4.05
0.965 hole	-2.07	16	5.44	3.61
0.584 hole	-3.42	16	5.10	3.32
0.584 wire	3.42	25	3.02	2.88
0.965 wire	2.07	25	3.29	2.93
1.575 wire	1.27	25	3.99	3.81
1.575 hole	-1.27	25	6.40	4.60
0.965 hole	-2.07	25	6.06	4.14
0.584 hole	-3.42	25	6.18	3.93

Table V - Continued

Specimen Diameter (mm)	Surface Curvature, 1/r (mm^{-1})	Oxidation Time (hours)	Mean Grain Intercept for the Columnar Layer, $\bar{\lambda}_{COL}$ ($\times 10^{-3}$ mm)	Mean Grain Intercept for the Equiaxed Layer, $\bar{\lambda}_{EQ}$ ($\times 10^{-3}$ mm)
0.584 wire	3.42	36	3.97	3.74
0.965 wire	2.07	36	4.17	3.76
1.575 wire	1.27	36	4.69	4.79
1.575 hole	-1.27	36	7.47	5.74
0.965 hole	-2.07	36	7.04	4.95
0.584 hole	-3.42	36	7.01	4.91
0.584 wire	3.42	49	3.82	3.42
0.965 wire	2.07	49	4.17	4.07
1.575 wire	1.27	49	5.00	4.77
1.575 hole	-1.27	49	8.23	6.43
0.965 hole	-2.07	49	8.19	5.75
0.584 hole	-3.42	49	8.10	5.72

Table VI

Equiaxed Fraction of the Total Scale Thickness for Wire and Hole Nickel 270 Specimens

Specimen Diameter (mm)	Surface Curvature, $1/r_1$ (mm^{-1})	Oxidation Time (hours)	Equiaxed Fraction of Total Scale Thickness, X_{EQ}/X
0.584 wire	3.42	4	0.41
0.965 wire	2.07	4	0.44
1.575 wire	1.27	4	0.45
1.575 hole	-1.27	4	0.37
0.965 hole	-2.07	4	0.47
0.584 hole	-3.42	4	0.52
0.584 wire	3.42	9	0.33
0.965 wire	2.07	9	0.36
1.575 wire	1.27	9	0.38
1.575 hole	-1.27	9	0.42
0.965 hole	-2.07	9	0.46
0.584 hole	-3.42	9	0.53

Table VI - Continued

Specimen Diameter (mm)	Surface Curvature, 1/r (mm^{-1})	Oxidation Time (hours)	Equiaxed Fraction of Total Scale Thickness, X_{EQ}/X
0.584 wire	3.42	16	0.31
0.965 wire	2.07	16	0.33
1.575 wire	1.27	16	0.37
1.575 hole	-1.27	16	0.43
0.965 hole	-2.07	16	0.49
0.584 hole	-3.42	16	0.53
0.584 wire	3.42	25	0.37
0.965 wire	2.07	25	0.36
1.575 wire	1.27	25	0.36
1.575 hole	-1.27	25	0.45
0.965 hole	-2.07	25	0.48
0.584 hole	-3.42	25	0.53

Table VI - Continued

Specimen Diameter (mm)	Surface Curvature, 1/r (mm^{-1})	Oxidation Time (hours)	Equiaxed Fraction of Total Scale Thickness, X_{EQ}/X
0.584 wire	3.42	36	0.37
0.965 wire	2.07	36	0.39
1.575 wire	1.27	36	0.41
1.575 hole	-1.27	36	0.44
0.965 hole	-2.07	36	0.49
0.584 hole	-3.42	36	0.52
0.584 wire	3.42	49	0.35
0.965 wire	2.07	49	0.40
1.575 wire	1.27	49	0.42
1.575 hole	-1.27	49	0.46
0.965 hole	-2.07	49	0.49
0.584 hole	-3.42	49	0.53

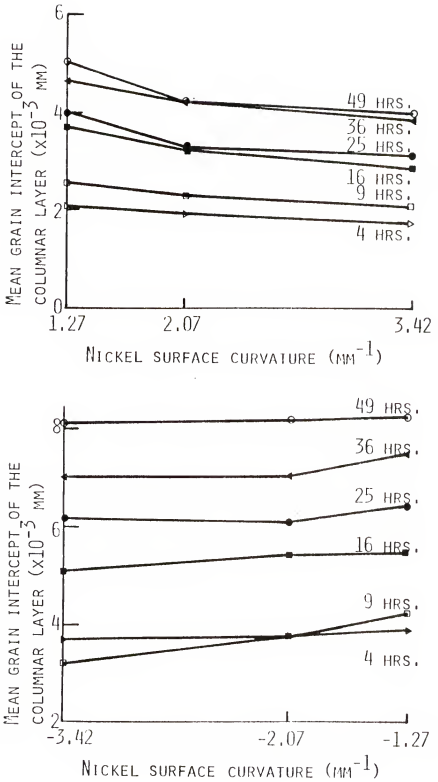

Figure 10. Mean grain intercept of the columnar layer, $\bar{\lambda}_{COL}$, versus nickel surface curvature, 1/r, (a) Wire specimens, (b) Hole specimens.

the columnar layer increases (Figure 10a), but as the hole surface curvature decreases, the mean grain intercept of the columnar layer decreases (Figure 10b). Comparison of Figure 9 (average, total scale thickness versus nickel surface curvature for wires) and Figure 10a reveals that an increase in $\overline{\lambda}_{COL}$ is coordinated with an increase in total scale thickness over the same variation in wire surface curvature. Similar comparison of Figure 9 (average, total scale thickness versus nickel surface curvature for holes) and Figure 10b reveals that an increase in $\overline{\lambda}_{COL}$ is not coordinated with an increase in total scale thickness over the same variation in hole surface curvature.

Results similar to those found for the mean grain intercept of the columnar layer are obtained for the mean grain intercept of the equiaxed layer. The $\overline{\lambda}_{EQ}$ data are plotted versus nickel surface curvature in Figure 11.

A linear dependence is found at all oxidation times when the ratio of equiaxed layer thickness to total scale thickness, X_{EQ}/X, is plotted against nickel surface curvature, Figure 12. As the nickel surface curvature decreases, the equiaxed layer becomes a monotonically increasing fraction of the total scale thickness.

One not so apparent effect of nickel surface curvature upon NiO microstructure involves the ratio of columnar layer thickness to the mean grain intercept of the columnar grains, $X_{COL}/\overline{\lambda}_{COL}$. The "columnarity" values of the outer

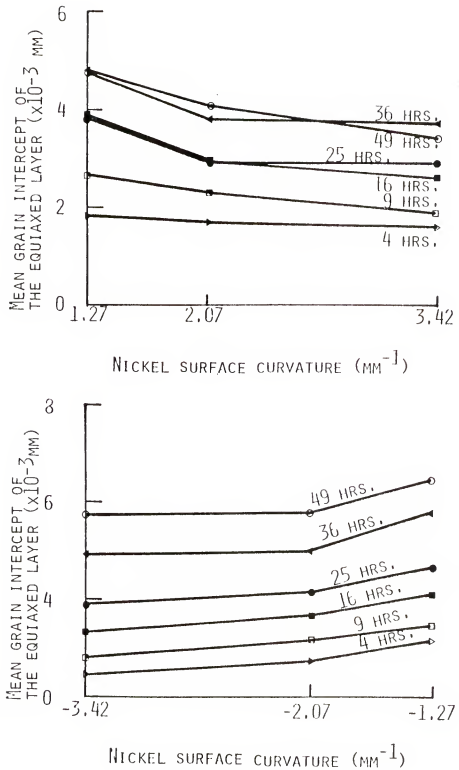

Figure 11. Mean grain intercept of the equiaxed layer, $\bar{\lambda}_{EQ}$, versus nickel surface curvature, 1/r, (a) Wire specimens, (b) Hole specimens.

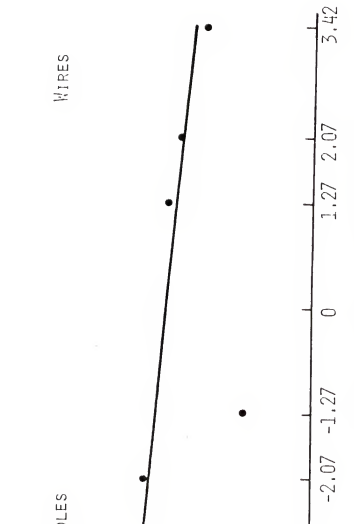

Figure 12. Equiaxed fraction of total scale thickness, X_{EQ}/X, versus nickel surface curvature, 1/r.

(a) Specimens oxidized for 4 hours.

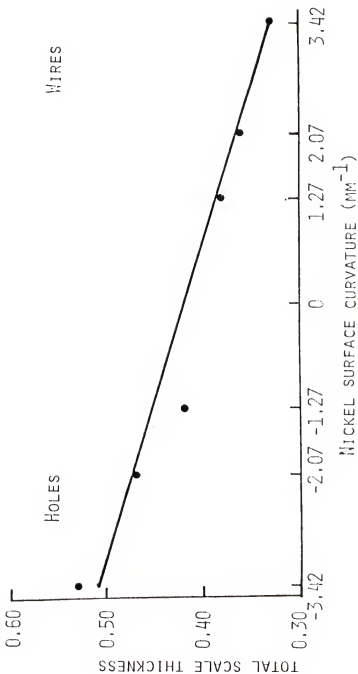

Figure 12. (continued).

(b) Specimens oxidized for 9 hours.

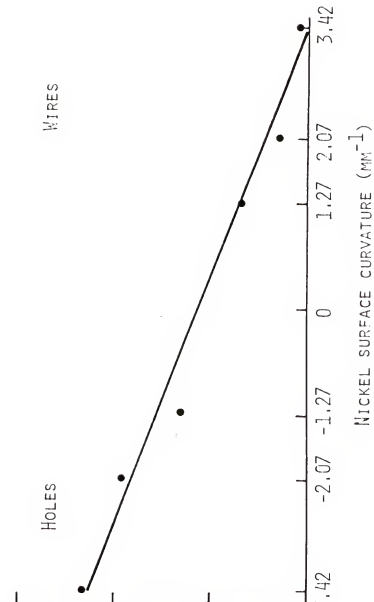

Figure 12. (continued).

(c) Specimens oxidized for 16 hours.

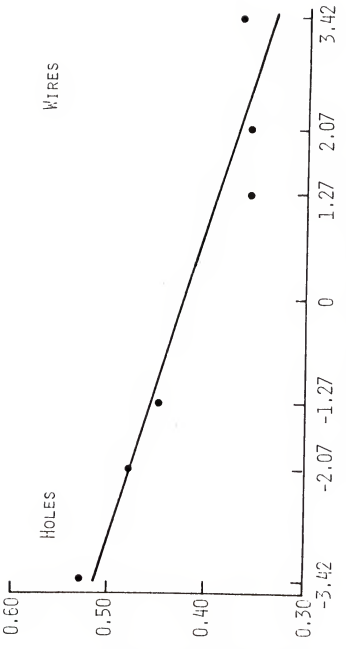

Figure 12. (continued).

(d) Specimens oxidized for 25 hours.

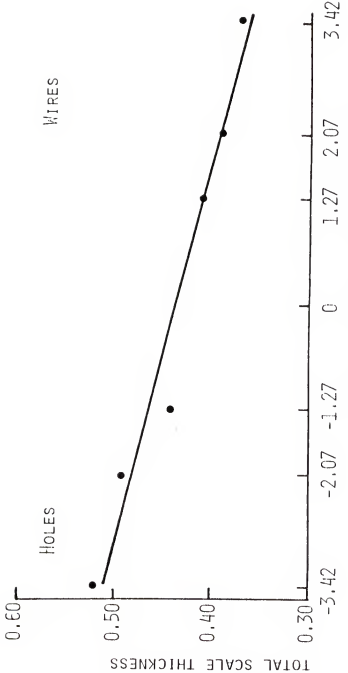

Figure 12. (continued).

(e) Specimens oxidized for 36 hours.

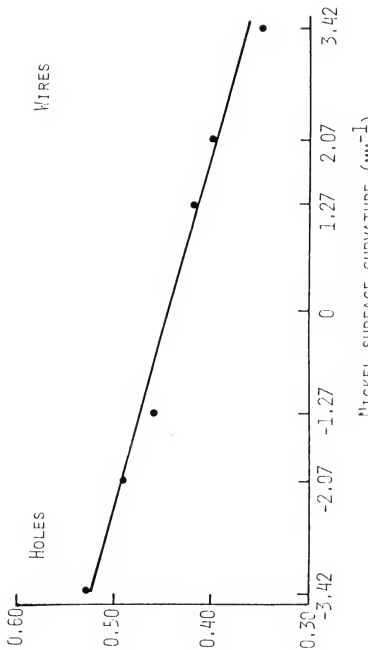

Figure 12. (continued).

(f) Specimens oxidized for 49 hours.

layer are presented in Table VII and graphed versus nickel surface curvature in Figure 13. The curves, at all oxidation times, indicate that a linear dependence of columnarity upon nickel surface curvature exists and that columnarity decreases with decreasing nickel surface curvature.

3.1.3. Examination of the Best-Fit Scale Thickening Curves for Wire and Hole Specimens at Short Oxidation Times

Best-fit curves, of the form $X = At^B + C$,* were calculated from the total scale thickness and columnar layer thickness data of Tables III and VIII. Extrapolation of these curves to zero oxidation time is shown in Figures 14 and 15. It is an important observation that all the curves intersect the oxidation time axis at positive values and do so in decreasing order from the smallest diameter wire (highest surface curvature) to the smallest diameter hole (lowest surface curvature).

3.2. Growth of NiO Upon Flat Specimens

Oxidation temperature also influences both the total scale thickness and microstructure of NiO, as illustrated by Figure 6. These photomicrographs reveal that the NiO scale formed at 1000°C is thicker than that formed at 800°C,

---

*X is scale thickness of either the total or columnar layer in microns, t is oxidation time in hours and A, B and C are constants.

Table VII

Columnarity Values of the Outer Layer of NiO Formed Upon Wire and Hole Nickel 270 Specimens

Specimen Diameter (mm)	Surface Curvature, $1/r$ (mm^{-1})	Oxidation Time (hours)	Columnarity of the Outer Layer, $X_{COL}/\bar{X}_{COL}$
0.584 wire	3.42	4	2.80
0.965 wire	2.07	4	2.60
1.575 wire	1.27	4	2.76
1.575 hole	-1.27	4	2.47
0.965 hole	-2.07	4	2.38
0.584 hole	-3.42	4	2.11
0.584 wire	3.42	9	4.32
0.965 wire	2.07	9	3.92
1.575 wire	1.27	9	3.54
1.575 hole	-1.27	9	3.05
0.965 hole	-2.07	9	2.80
0.584 hole	-3.42	9	2.70

Table VII - Continued

Specimen Diameter (mm)	Surface Curvature, 1/r (mm^{-1})	Oxidation Time (hours)	Columnarity of the Outer Layer, $X_{COL}/\bar{\lambda}_{COL}$
0.584 wire	3.42	16	4.28
0.965 wire	2.07	16	3.91
1.575 wire	1.27	16	3.24
1.575 hole	-1.27	16	3.05
0.965 hole	-2.07	16	2.58
0.584 hole	-3.42	16	2.72
0.584 wire	3.42	25	3.98
0.965 wire	2.07	25	4.08
1.575 wire	1.27	25	3.75
1.575 hole	-1.27	25	2.63
0.965 hole	-2.07	25	2.88
0.584 hole	-3.42	25	2.63

Table VII - Continued

Specimen Diameter (mm)	Surface Curvature, $1/r$ (mm^{-1})	Oxidation Time (hours)	Columnarity of the Outer Layer, $X_{COL}/\bar{X}_{COL}$
0.584 wire	3.42	36	3.60
0.965 wire	2.07	36	3.49
1.575 wire	1.27	36	3.40
1.575 hole	-1.27	36	2.89
0.965 hole	-2.07	36	2.97
0.584 hole	-3.42	36	2.86
0.584 wire	3.42	49	4.55
0.965 wire	2.07	49	4.10
1.575 wire	1.27	49	3.55
1.575 hole	-1.27	49	2.69
0.965 hole	-2.07	49	2.66
0.584 hole	-3.42	49	2.59

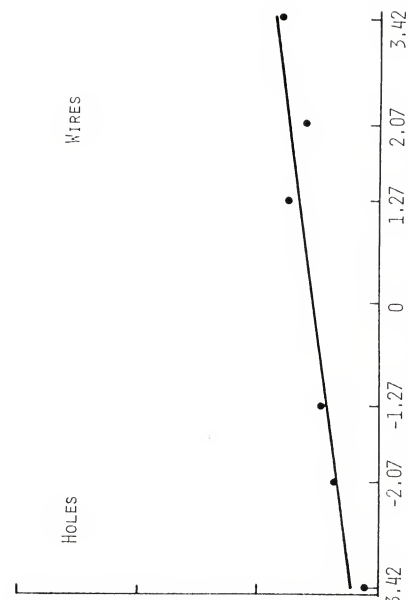

Figure 13. Columnarity of the outer layer, $X_{COL}/\overline{X}_{COL}$, versus nickel surface curvature, 1/r.

(a) Specimens oxidized for 4 hours.

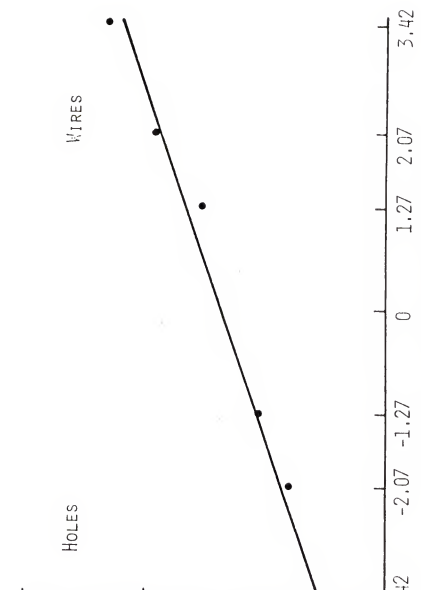

Figure 13. (continued).

(b) Specimens oxidized for 9 hours.

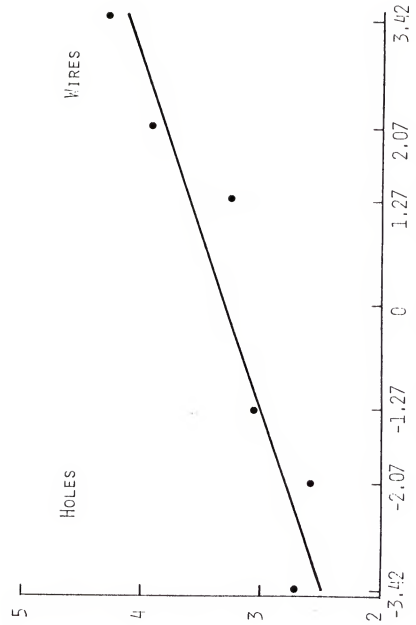

Figure 13. (continued).

(c) Specimens oxidized for 16 hours.

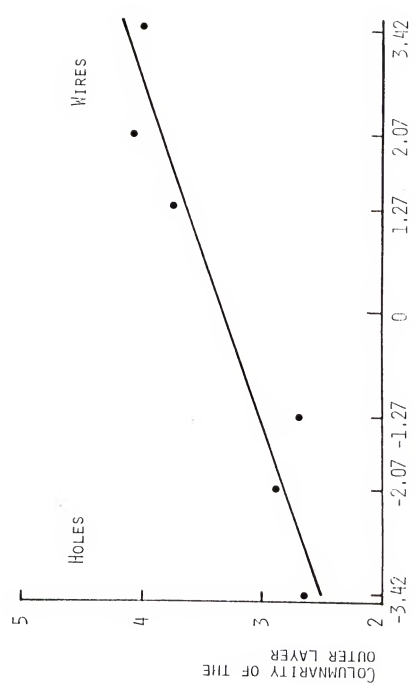

Figure 13. (continued).

(d) Specimens oxidized for 25 hours.

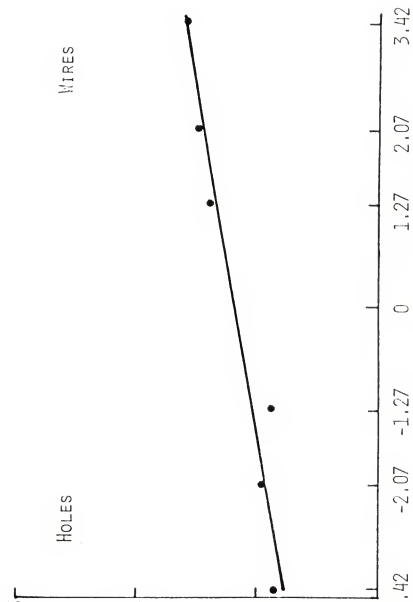

Figure 13. (continued).

(e) Specimens oxidized for 36 hours.

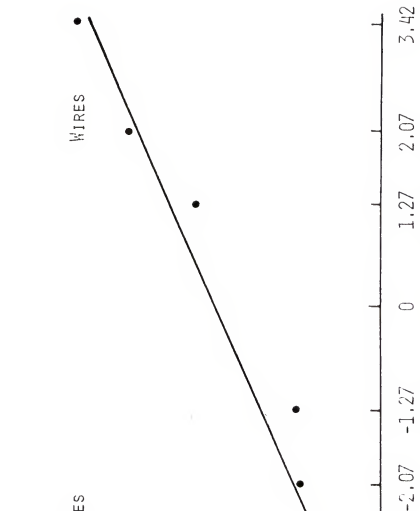

Figure 13. (continued).

(f) Specimens oxidized for 49 hours.

Table VIII

Columnar Layer Thickness Measurements for Wire and Hole Nickel 270 Specimens

Specimen Diameter (mm)	Surface Curvature, $1/r$ (mm^{-1})	Oxidation Time (hours)	Columnar Layer Thickness, X_{COL} ($\times 10^{-3}$ mm)
0.584 wire	3.42	4	4.92 ± 0.59
0.965 wire	2.07	4	4.99 ± 0.42
1.575 wire	1.27	4	5.54 ± 0.45
1.575 hole	-1.27	4	10.45 ± 0.64
0.965 hole	-2.07	4	9.01 ± 0.79
0.584 hole	-3.42	4	7.80 ± 0.56
0.584 wire	3.42	9	8.72 ± 0.65
0.965 wire	2.07	9	8.95 ± 0.75
1.575 wire	1.27	9	9.13 ± 0.77
1.575 hole	-1.27	9	11.83 ± 0.91
0.965 hole	-2.07	9	10.63 ± 1.04
0.584 hole	-3.42	9	8.74 ± 0.63

Table VIII - Continued

Specimen Diameter (mm)	Surface Curvature, $1/r$ (mm^{-1})	Oxidation Time (hours)	Columnar Layer Thickness, X_{COL} ($\times 10^{-3}$ mm)
0.584 wire	3.42	16	12.21 ± 0.57
0.965 wire	2.07	16	12.55 ± 0.55
1.575 wire	1.27	16	12.00 ± 0.71
1.575 hole	-1.27	16	16.64 ± 1.40
0.965 hole	-2.07	16	14.01 ± 1.15
0.584 hole	-3.42	16	13.86 ± 1.31
0.584 wire	3.42	25	12.03 ± 0.84
0.965 wire	2.07	25	13.43 ± 0.83
1.575 wire	1.27	25	14.95 ± 1.13
1.575 hole	-1.27	25	16.84 ± 1.09
0.965 hole	-2.07	25	17.44 ± 1.41
0.584 hole	-3.42	25	16.25 ± 1.42

Table VIII - Continued

Specimen Diameter (mm)	Surface Curvature, $1/r$ (mm^{-1})	Oxidation Time (hours)	Columnar Layer Thickness, X_{COL} ($\times 10^{-3}$ mm)
0.584 wire	3.42	36	14.28 ± 1.06
0.965 wire	2.07	36	14.54 ± 0.65
1.575 wire	1.27	36	15.96 ± 0.98
1.575 hole	-1.27	36	21.57 ± 1.56
0.965 hole	-2.07	36	20.93 ± 1.33
0.584 hole	-3.42	36	20.02 ± 0.83
0.584 wire	3.42	49	17.40 ± 1.73
0.965 wire	2.07	49	17.08 ± 0.81
1.575 wire	1.27	49	17.77 ± 0.77
1.575 hole	-1.27	49	22.13 ± 1.73
0.965 hole	-2.07	49	21.83 ± 1.35
0.584 hole	-3.42	49	20.98 ± 1.63

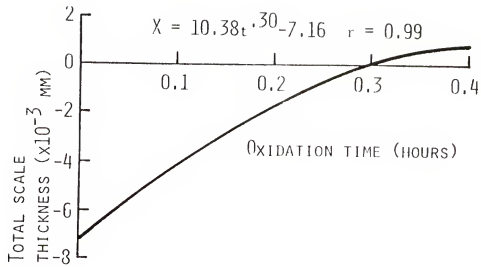

(a) 0.584 mm diameter wire specimen.

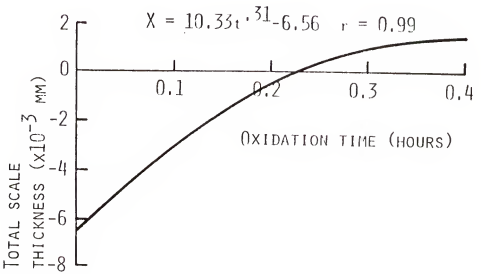

(b) 0.965 mm diameter wire specimen.

Figure 14. Total scale thickness, X, versus oxidation time, t, extrapolated to t = 0 for wire and hole specimens.

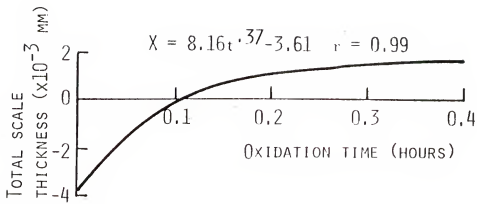

(c) 1.575 mm diameter wire specimen.

Figure 14. (continued).

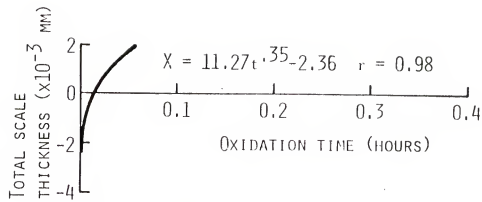

(d) 1.575 mm diameter hole specimen.

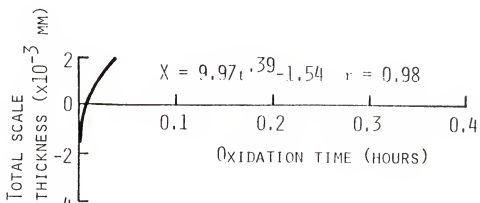

(e) 0.965 mm diameter hole specimen.

Figure 14. (continued).

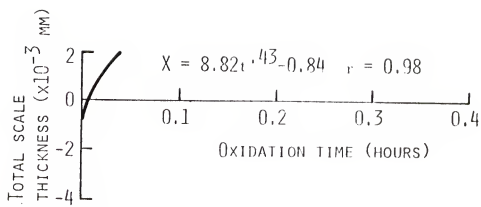

(f) 0.584 mm diameter hole specimen.

Figure 14. (continued).

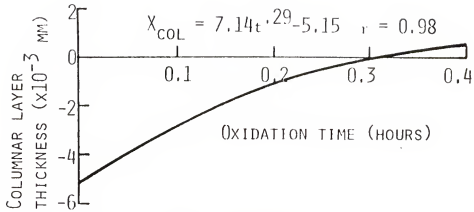

(a) 0.584 mm diameter wire specimen.

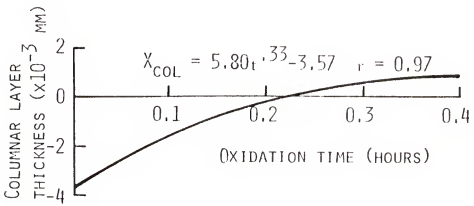

(b) 0.965 mm diameter wire specimen.

Figure 15. Columnar layer thickness, X_{COL}, versus oxidation time, t, extrapolated to t = 0 for wire and hole specimens.

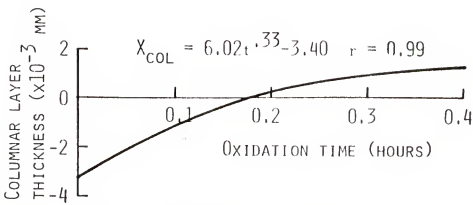

(c) 1.575 mm wire specimen.

Figure 15. (continued).

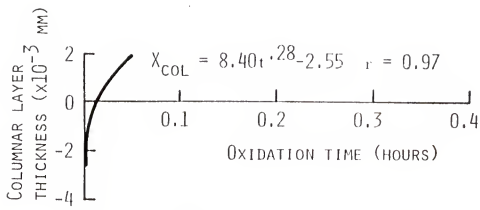

(d) 1.575 mm diameter hole specimen.

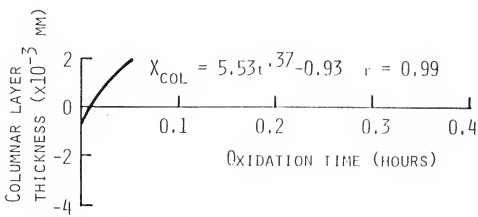

(e) 0.965 mm diameter hole specimen.

Figure 15. (continued).

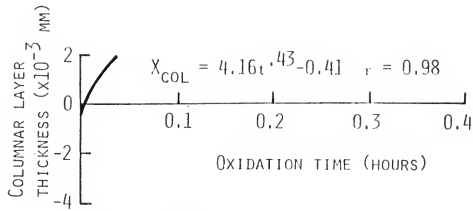

(f) 0.584 mm diameter hole specimen.

Figure 15. (continued).

the NiO scale formed at 800°C is finer-grained than that formed at 1000°C and the equiaxed layer thickness is a larger fraction of the total scale thickness at 800°C than at 1000°C.

3.2.1. Total Scale Thickness of NiO Formed Upon Flat Specimens

Total NiO scale thickness data for flat specimens oxidized at 1000°C and 800°C are recorded in Table IX along with their respective 95% confidence intervals. These data, when plotted against oxidation time, result in the scale thickening curves of Figure 16. The kinetic equations for these best-fit curves and their corresponding correlation coefficients are given. Thicker NiO scales are formed at the higher oxidation temperature.

3.2.2. Microstructure of NiO Formed Upon Flat Specimens

Qualitative correlation between total NiO scale thickness and NiO microstructure is found from examination of Figure 6. A coarse-grained, thick oxide develops at 1000°C compared to a fine-grained, thin oxide at 800°C. This observation of coordination betwen NiO grain growth and NiO scale growth upon flat specimens is in agreement with earlier work [18, 19].

Another microstructural feature of NiO influenced by oxidation temperature is the relative thickness of scale layers, Table X. When the equiaxed fraction of total scale thickness, X_{EQ}/X, is plotted versus oxidation time, Figure

Table IX

Total NiO Scale Thickness Measurements for Flat Nickel 270 Specimens

Specimen Oxidation Temperature (°C)	Oxidation Time (hours)	Total Scale Thickness, X ($\times 10^{-3}$ mm)
1000	4	10.62 ± 0.60
800	4	--
1000	9	14.70 ± 0.92
800	9	8.36 ± 0.48
1000	16	20.54 ± 0.98
800	16	10.01 ± 0.39
1000	25	22.88 ± 1.18
800	25	12.19 ± 0.34
1000	36	29.18 ± 1.30
800	36	13.54 ± 0.46
1000	49	30.63 ± 0.91
800	49	14.95 ± 0.40

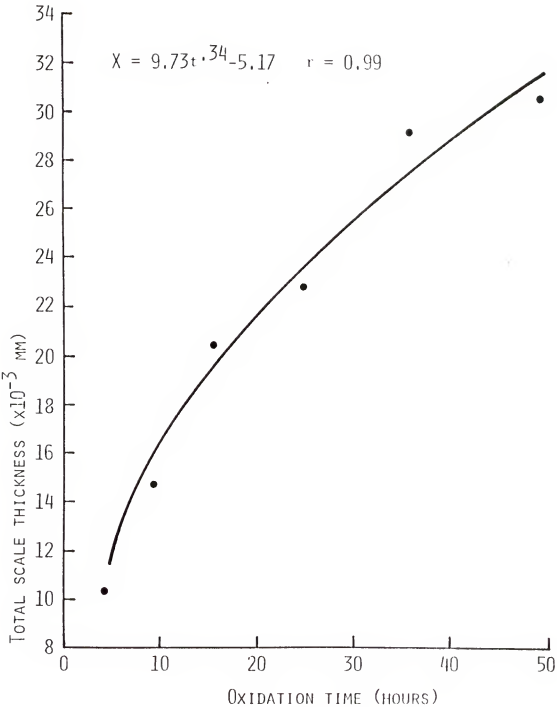

Figure 16. Total scale thickness, X, versus oxidation time, t, for flat specimens.

(a) Specimens oxidized at 1000°C.

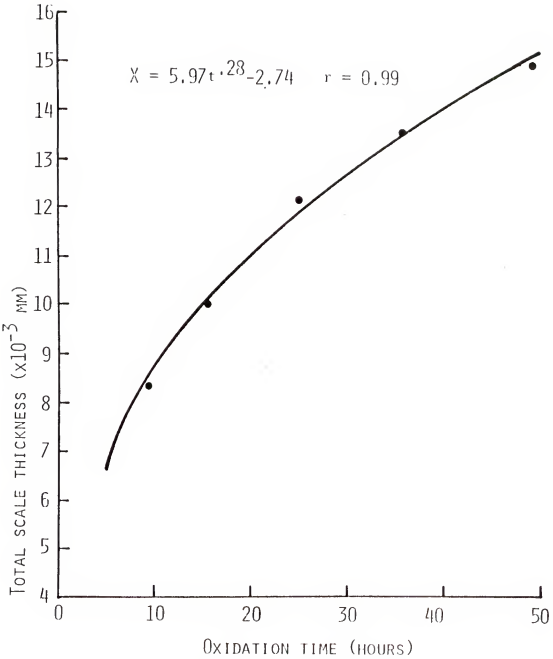

Figure 16. (continued).

(b) Specimens oxidized at 800°C.

Table X

Equiaxed Fraction of the Total Scale Thickness for Flat Nickel 270 Specimens

Specimen Oxidation Temperature (°C)	Oxidation Time (hours)	Equiaxed Fraction of Total Scale Thickness, X_{EQ}/X
1000	4	0.39
800	4	--
1000	9	0.41
800	9	0.56
1000	16	0.40
800	16	0.55
1000	25	0.36
800	25	0.56
1000	36	0.36
800	36	0.56
1000	49	0.35
800	49	0.55

17, it is clearly seen that a smaller fraction of the total scale thickness consists of equiaxed grains after oxidation at 1000°C than at 800°C.

3.2.3. Examination of the Best-Fit Scale Thickening Curves for Flat Specimens at Short Oxidation Times

Best-fit curves, of the form $X = At^B + C$,* were calculated from the total scale thickness and columnar layer thickness data of Tables IX and XI. Extrapolation of these curves to zero oxidation time is shown in Figures 18 and 19. As was the case for wire and hole specimens, all the curves intersect the oxidation time axis at positive values. The 1000°C curves have larger intercepts than the corresponding 800°C curves.

*X is scale thickness of either the total or columnar layer in microns, t is oxidation time in hours and A, B and C are constants.

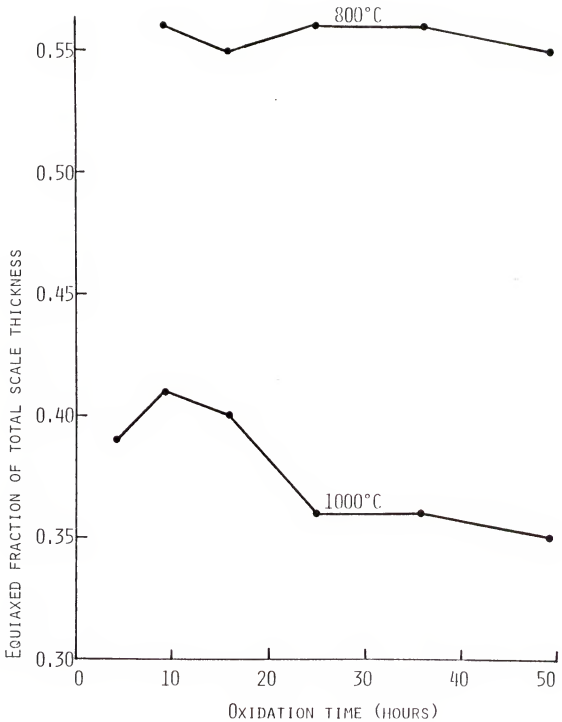

Figure 17. Equiaxed fraction of total scale thickness, X_{EQ}/X, versus oxidation time, t, for flat specimens.

Table XI

Columnar Layer Thickness Measurements for Flat Nickel 270 Specimens

Specimen Oxidation Temperature (°C)	Oxidation Time (hours)	Columnar Layer Thickness, X_{COL} ($\times 10^{-3}$ mm)
1000	4	6.48 ± 0.41
800	4	--
1000	9	8.60 ± 0.32
800	9	3.67 ± 0.51
1000	16	12.34 ± 0.49
800	16	4.52 ± 0.43
1000	25	14.64 ± 0.31
800	25	5.34 ± 0.40
1000	36	18.70 ± 0.76
800	36	5.99 ± 0.43
1000	49	19.82 ± 0.72
800	49	6.67 ± 0.38

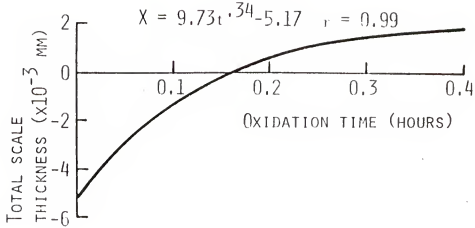

(a) Specimens oxidized at 1000°C.

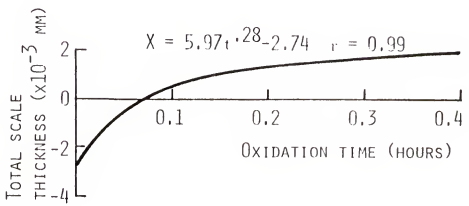

(b) Specimens oxidized at 800°C.

Figure 18. Total scale thickness, X, versus oxidation time, t, extrapolated to t = 0 for flat specimens.

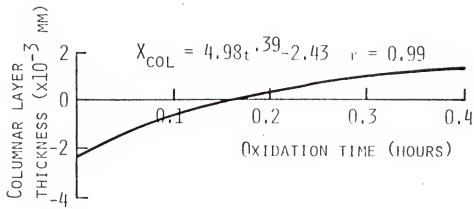

(a) Specimens oxidized at 1000°C.

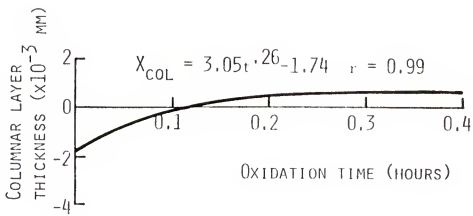

(b) Specimens oxidized at 800°C.

Figure 19. Columnar layer thickness, X_{COL}, versus oxidation time, t, extrapolated to t = 0 for flat specimens.

CHAPTER IV

DISCUSSION OF THE EXPERIMENTAL RESULTS

In order to define the scope of the discussion that follows, the principal experimental facts that can now be considered to have been established will be summarized.

1. Nucleation of the first oxide occurs along grain boundaries of the metal [62-64]. Many NiO nuclei form upon a single nickel grain [14, 22] and begin to grow by the addition of oxygen ions at their edges [66].
2. The transport of nickel through the NiO scale involves the diffusion of nickel ions outward through the NiO lattice [35, 37].
3. Evidence for oxygen diffusion has been supplied by tracer analysis [105] wherein nickel was oxidized first in a pure ^{16}O atmosphere and then in an ^{16}O plus ^{18}O atmosphere. Subsequent analysis verified the presence of ^{18}O all the way to the metal/oxide interface.
4. The transport of oxygen through the NiO scale involves the diffusion of oxygen ions inward along NiO grain boundaries [38, 39].
5. The formation of new NiO occurs along a common reaction interface for nickel and oxygen ions--the NiO grain

boundaries--as well as at the external surface and metal/oxide interface [18].

6. Lateral, compressive stresses are generated within the scale during oxidation [7, 16, 48-52].
7. Plastic deformation of NiO occurs during oxidation [18, 13, 16, 32, 58-60].
8. Ridges of NiO located on the external surface, their spacing corresponding to the lateral spacing of the columnar grain boundary intersections with the external surface, appear early in oxidation [18]. With continued growth these ridges become broader and less distinct until the external surface becomes faceted.
9. NiO grain growth occurs in quantitative proportion to NiO scale growth [8, 18, 19, 26-29].
10. NiO scale growth does not occur in the absence of NiO grain growth, nor is grain growth observed without oxidation [18].

The above facts reveal that NiO scale growth, NiO grain growth, stress generation within the scale and plastic deformation of the oxide are mutually interdependent components of the high-temperature oxidation of nickel. Therefore, any variable of the oxidation process affecting any one of these components, must also affect the other three. The current research proposes that two such variables are the nickel surface curvature and the oxidation temperature.

4.1. The Effect of Nickel Surface Curvature Upon the High-Temperature Oxidation of Nickel

Oxidation of Nickel 270 wire and hole specimens at 1000°C has yielded the following results:

1. All scale thickening curves intersect the oxidation time axis at positive values and do so in decreasing order from the smallest diameter wire to the smallest diameter hole (i.e. an incubation period exists in all cases).
2. Two linear relationships exist between total scale thickness and nickel surface curvature--one for wire specimens and one for hole specimens. In each case, the total scale thickness increases linearly with decreasing nickel surface curvature, but the linear relationship found for hole specimens is displaced above that for wire specimens.
3. The NiO grain size, as measured by $\bar{\lambda}_{COL}$ and $\bar{\lambda}_{EQ}$, is larger upon hole specimens than upon wire specimens. Both $\bar{\lambda}_{COL}$ and $\bar{\lambda}_{EQ}$ increase as wire surface curvature decreases and decrease as hole surface curvature decreases.
4. The relative thickness of the equiaxed layer to the total scale thickness, X_{EQ}/X, increases linearly with decreasing nickel surface curvature.
5. The columnarity of the outer layer, $X_{COL}/\bar{\lambda}_{COL}$, decreases linearly with decreasing nickel surface curvature.

These results, when combined with the foregoing established facts, lead to a new model of the high-temperature oxidation of nickel.

4.1.1. Proposed Model of the High-Temperature Oxidation of Nickel

Nucleation of the first oxide begins along grain boundaries of the underlying metal [62.65] and spreads across the grains. These nuclei, formed upon nickel grains [14, 22], grow by the addition of oxygen ions at their edges until they impinge, one upon the other, and the nickel surface becomes completely covered by a thin film of NiO [66]. Following complete coverage of the metal, oxidation is controlled by the outward diffusion of nickel ions through the NiO lattice to the external surface, whereupon oxygen ions are contacted and new NiO is formed. During this initial, diffusion-controlled stage of oxidation, accretion of NiO upon the external surface develops a layer of columnar grains. Presently, oxygen ions diffusing inward along NiO grain boundaries meet nickel ions diffusing outward through the NiO lattice to form new NiO along a common reaction interface--the oxide grain boundaries. Gradually, after a sufficient columnar layer thickness is attained, a later stage of oxidation begins which is characterized by the onset of NiO grain boundary sweeping and the nucleation of new oxide grains at the metal/oxide interface. Scale growth during this later stage of oxidation occurs by swelling of the oxide, which causes a faster rate of oxidation than of

accretion of oxide upon the external surface (initial stage of oxidation). This two-stage oxidation process is shown schematically in Figure 20.

During the initial stage of oxidation the scale is composed of columnar grains which grow outward from the metal surface. New NiO is formed along the oxide grain boundaries which lie normal to the metal/oxide interface, thus creating a lateral "wedging effect" upon neighboring NiO grains and establishing compressive stresses within the scale. As long as the scale is relatively thin, any plastic response of the NiO to relieve these compressive stresses occurs by the outward extrusion of newly formed NiO along the oxide grain boundaries. Manifestation of this outward extrusion is shown in the scanning electron micrograph of Figure 21. Ridges of extruded oxide appear on the external surface having the same spacing as the intersection of columnar grain boundaries with the external surface.

The later stage of oxidation begins when the columnar layer of the NiO scale develops sufficient thickness so that outward extrusion of newly formed NiO is no longer energetically expedient. At this point, relief of the lateral, compressive stresses by plastic deformation involves the passage of shear across NiO grain boundaries, a circumstance which increases the local curvature of the grain boundaries [104]. Increased grain boundary curvature

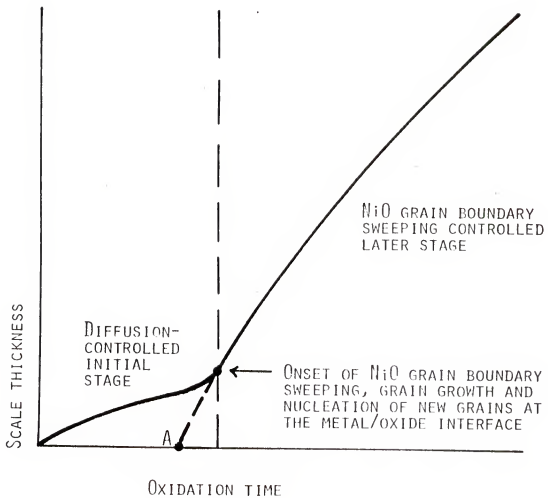

Figure 20. Schematic representation of the proposed two-stage oxidation model.

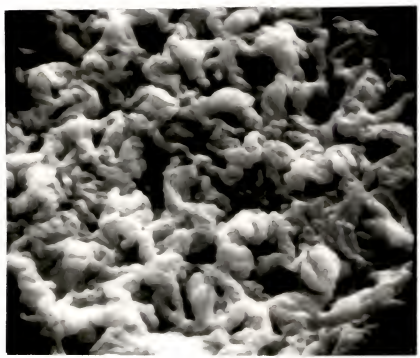

1000X

Figure 21. Scanning electron micrograph illustrating the surface morphology of NiO grown upon a flat Nickel 270 specimen at 800°C for 1 hour. Note the ridges of NiO along the oxide grain boundaries.

results in grain boundary sweeping and grain growth, under the influence of surface tension, in order to minimize NiO grain boundary surface area. The sweeping of NiO grain boundaries provides for a moving reaction front, whereupon nickel and oxygen ions meet to form new NiO, and for the distribution of newly formed oxide throughout the scale volume. This results in swelling of the oxide scale and in nucleation of new, NiO grains at the metal/oxide interface.

4.1.2. The Effect of Nickel Surface Curvature Upon the Proposed Model

Nickel surface curvature affects the proposed model of oxidation by controlling the onset of NiO grain boundary sweeping (later stage of oxidation). It is believed that the curvature of the oxidizing surface affects the lateral, compressive stresses generated during oxidation. This belief arises from the fact that as the nickel surface curvature decreases, the newly formed NiO must grow into progressively decreasing space, for a given scale thickness, thereby exerting a greater force upon neighboring NiO grains. Consequently, the onset of NiO grain boundary sweeping and nucleation of new NiO grains at the metal/oxide interface occurs earlier in oxidation as nickel surface curvature decreases. This trend applies continuously from sharply convex to sharply concave surface curvature.

Graphical support of this consequence is given by Figures 14 and 15, total scale thickness and columnar layer

thickness, respectively, versus oxidation time for wire and hole specimens. Examination of these curves reveals a consistent trend in the point at which they intersect the oxidation time axis. These intersections correspond to point A in Figure 20, the schematic representation of oxidation, and estimate the time during which diffusion-controlled growth of NiO occurs (initial stage) and before which NiO grain boundary sweeping begins (later stage). The value of each of these intercepts is shown as incubation time in Tables XII and XIII, as calculated from the kinetic equations for total scale thickness and columnar layer thickness, respectively. A decrease in the incubation time with decreasing nickel surface curvature results in each case. Thus, nickel surface curvature controls the onset of NiO grain boundary sweeping. As nickel surface curvature decreases, NiO grain boundary sweeping begins earlier in oxidation.

The incubation times calculated from the kinetic equations and presented in Tables XII and XIII should not be taken as the moment of onset of NiO grain boundary sweeping. These values merely indicate that NiO grain boundary sweeping begins earlier in oxidation as nickel surface curvature decreases.

4.1.3. The Effect of Nickel Surface Curvature Upon the Scale Thickening and Microstructural Evolution of NiO

Support for the proposed model of the high-temperature oxidation of nickel is also found in the effect of nickel

Table XII

Incubation Times for NiO Grown Upon Wire and Hole Nickel 270 Specimens Calculated From Total Scale Thickness Data

Specimen Diameter (mm)	Surface Curvature, $1/r$ (mm^{-1})	Incubation Time (hours)
0.584 wire	3.42	2.90×10^{-1}
0.965 wire	2.07	2.31×10^{-1}
1.575 wire	1.27	1.10×10^{-1}
1.575 hole	-1.27	1.15×10^{-2}
0.965 hole	-2.07	8.32×10^{-3}
0.584 hole	-3.42	4.22×10^{-3}

Table XIII

Incubation Times for NiO Grown Upon Wire and Hole Nickel 270 Specimens Calculated From Columnar Layer Thickness Data

Specimen Diameter (mm)	Surface Curvature, $1/r$ (mm^{-1})	Incubation Time (hours)
0.584 wire	3.42	3.24×10^{-1}
0.965 wire	2.07	2.30×10^{-1}
1.575 wire	1.27	1.77×10^{-1}
1.575 hole	-1.27	1.42×10^{-2}
0.965 hole	-2.07	8.08×10^{-3}
0.584 hole	-3.42	4.57×10^{-3}

surface curvature upon the scale thickening and microstructural evolution of NiO. These effects can be explained in terms of the control of nickel surface curvature over the onset of NiO grain boundary sweeping.

4.1.3.1. Scale thickening upon wire and hole specimens

Scale thickening during the later stage of oxidation is enhanced over that during the initial stage because NiO grain boundary sweeping causes swelling of the oxide, not merely accretion of oxide upon the external surface. It follows that the earlier the onset of NiO grain boundary sweeping, the thicker is the total NiO scale. Therefore, as nickel surface curvature decreases, the total scale thickness of NiO should increase. Examination of Figure 9, average, total scale thickness for the six oxidation times versus nickel surface curvature, substantiates this deduction.

4.1.3.2. Microstructural evolution of NiO upon wire and hole specimens

The microstructural evolution of NiO formed upon wire and hole specimens is evaluated in three ways: (1) mean grain intercept determinations; (2) relative thickness of scale layers; and (3) columnarity of the outer layer. These quantitative, microstructural analyses are points of discussion in the following paragraphs.

Mean grain intercept values for both the columnar and equiaxed layers of NiO are found to increase with oxidation time, regardless of the specimen surface curvature, Table V.

This behavior substantiates the fact that NiO scale growth does not occur without NiO grain growth [18, 19]. With this in mind, and since total scale thickness increases with decreasing nickel surface curvature, it should be expected that the NiO grain size increases as the nickel surface curvature decreases. In fact, the data of Table V indicate that the NiO grain size is larger upon hole specimens than upon wire specimens. However, graphs of the mean grain intercept versus nickel surface curvature for the columnar layer, Figure 10, and the equiaxed layer, Figure 11, show this expectation to hold true for wire specimens but not for hole specimens. Explanation involves the initial size of NiO grains, which is the same on all wire specimens, but varies from one hole specimen to another.

To determine the correlation between the initial grain size of NiO and the nickel surface curvature, the NiO grain boundary surface area per unit volume of scale, $S_{V\ TOTAL}$, was calculated for each condition of oxidation. $S_{V\ TOTAL}$ is inversely proportional to the NiO grain size and, when extrapolated to zero total scale thickness, is inversely proportional to the initial NiO grain size. The method of calculation is outlined in Figure 22 and the $S_{V\ TOTAL}$ values, thus obtained, are recorded in Table XIV. When these data for wire specimens are plotted against total scale thickness, Figure 23, no evidence of an effect of wire surface curvature upon $S_{V\ TOTAL}$ can be found. Yet, when the data for hole

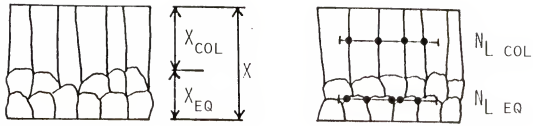

$$S_{V\ COL} = \frac{\pi}{2} N_{L\ COL} X_{COL}$$

$$S_{V\ COL} = \frac{\pi}{2} \frac{1}{\bar{\lambda}_{COL}} X_{COL}$$

$$S_{V\ EQ} = 2N_{L\ EQ} = 2 \frac{1}{\bar{\lambda}_{EQ}}$$

$$S_{V\ TOTAL} = S_{V\ COL}\left(1 - \frac{X_{EQ}}{X}\right) + S_{V\ EQ}\left(\frac{X_{EQ}}{X}\right)$$

WHERE
- X_{COL} - COLUMNAR LAYER THICKNESS
- X_{EQ} - EQUIAXED LAYER THICKNESS
- $N_{L\ COL}$ - NUMBER OF NiO GRAIN BOUNDARY INTERCEPTS PER UNIT LENGTH IN THE COLUMNAR LAYER
- $N_{L\ EQ}$ - NUMBER OF NiO GRAIN BOUNDARY INTERCEPTS PER UNIT LENGTH IN THE EQUIAXED LAYER
- $\bar{\lambda}_{COL}$ - MEAN GRAIN INTERCEPT OF COLUMNAR GRAINS
- $\bar{\lambda}_{EQ}$ - MEAN GRAIN INTERCEPT OF EQUIAXED GRAINS
- $S_{V\ COL}$ - NiO GRAIN BOUNDARY SURFACE AREA PER UNIT VOLUME OF COLUMNAR GRAINS
- $S_{V\ EQ}$ - NiO GRAIN BOUNDARY SURFACE AREA PER UNIT VOLUME OF EQUIAXED GRAINS
- $S_{V\ TOTAL}$ - NiO GRAIN BOUNDARY SURFACE AREA PER UNIT VOLUME OF SCALE

Figure 22. Method of calculating the NiO grain boundary surface area per unit volume of scale, $S_{V\ TOTAL}$.

Table XIV

NiO Grain Boundary Surface Area Per Unit Volume of Scale for Wire and Hole Nickel 270 Specimens

Specimen Diameter (mm)	Surface Curvature, 1/r (mm^{-1})	Oxidation Time (hours)	Total Scale Thickness, X ($\times 10^{-3}$ mm)	NiO Grain Boundary Surface Area Per Unit Volume of Scale, $S_{V\ TOTAL}$ (mm^2/mm^3)
0.584 wire	3.42	4	8.33	506.83
0.965 wire	2.07	4	9.00	521.48
1.575 wire	1.27	4	10.07	506.38
1.575 hole	-1.27	4	16.53	239.24
0.965 hole	-2.07	4	17.08	345.08
0.584 hole	-3.42	4	16.32	422.79
0.584 wire	3.42	9	13.09	354.34
0.965 wire	2.07	9	14.05	320.75
1.575 wire	1.27	9	14.69	292.25
1.575 hole	-1.27	9	20.39	246.38
0.965 hole	-2.07	9	19.79	292.18
0.584 hole	-3.42	9	18.68	383.60

Table XIV - Continued

Specimen Diameter (mm)	Surface Curvature, 1/r (mm^{-1})	Oxidation Time (hours)	Total Scale Thickness, X ($\times 10^{-3}$ mm)	NiO Grain Boundary Surface Area Per Unit Volume of Scale, $S_{V\ TOTAL}$ (mm^2/mm^3)
0.584 wire	3.42	16	17.75	243.34
0.965 wire	2.07	16	18.71	225.21
1.575 wire	1.27	16	18.94	195.61
1.575 hole	-1.27	16	29.08	213.44
0.965 hole	-2.07	16	27.42	271.56
0.584 hole	-3.42	16	29.78	320.01
0.584 wire	3.42	25	19.05	259.24
0.965 wire	2.07	25	21.06	248.90
1.575 wire	1.27	25	23.57	190.96
1.575 hole	-1.27	25	30.61	195.77
0.965 hole	-2.07	25	33.53	232.75
0.584 hole	-3.42	25	34.75	272.24

Table XIV - Continued

Specimen Diameter (mm)	Surface Curvature, 1/r (mm^{-1})	Oxidation Time (hours)	Total Scale Thickness, X ($\times 10^{-3}$ mm)	NiO Grain Boundary Surface Area Per Unit Volume of Scale, $S_{V_2 TOTAL}$ (mm^2/mm^3)
0.584 wire	3.42	36	22.58	199.66
0.965 wire	2.07	36	23.90	210.04
1.575 wire	1.27	36	27.01	175.35
1.575 hole	-1.27	36	38.81	156.66
0.965 hole	-2.07	36	41.03	198.38
0.584 hole	-3.42	36	42.02	215.35
0.584 wire	3.42	49	26.90	207.65
0.965 wire	2.07	49	28.56	199.86
1.575 wire	1.27	49	30.76	179.64
1.575 hole	-1.27	49	40.99	144.82
0.965 hole	-2.07	49	42.77	173.64
0.584 hole	-3.42	49	44.66	187.41

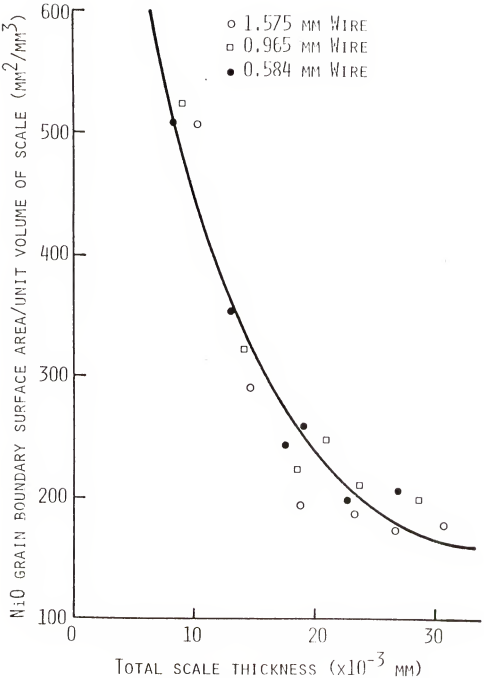

Figure 23. NiO grain boundary surface area per unit volume of scale, $S_{V\ TOTAL}$, versus total scale thickness, X, for wire specimens.

specimens are similarly plotted, Figure 24, a significant effect of hole surface curvature upon $S_{V\ TOTAL}$ is found. Apparently, the initial grain size of NiO decreases with decreasing hole surface curvature (decreasing hole diameter). Consequently, an increase in the mean grain intercept values with decreasing hole surface curvature may not occur even though the total scale thickness increases.

Further substantiation of an uncontrolled difference in the oxidation behavior of wire and hole specimens is found in Figure 9, average, total scale thickness for the six oxidation times versus nickel surface curvature. Two distinct and parallel linear relationships are seen which suggest the existence of an oxidation variable(s) unique to wire and hole specimens. Perhaps, due to different gas flow characteristics around each specimen, the concentration of impurities on the metal surface is greater upon the hole specimens (closed oxidizing surfaces) than upon wire specimens (open oxidizing surfaces). A refinement of the initial NiO grain size formed upon hole specimens would result due to the presence of more nucleation sites. And, as Graham et al. [29] determined, a finer-grained oxide thickens faster than a coarser-grained oxide.

The relative thickness of scale layers is affected by the onset of NiO grain boundary sweeping. The earlier NiO grain boundary sweeping begins, the thinner is the columnar layer developed during the initial stage of oxidation and

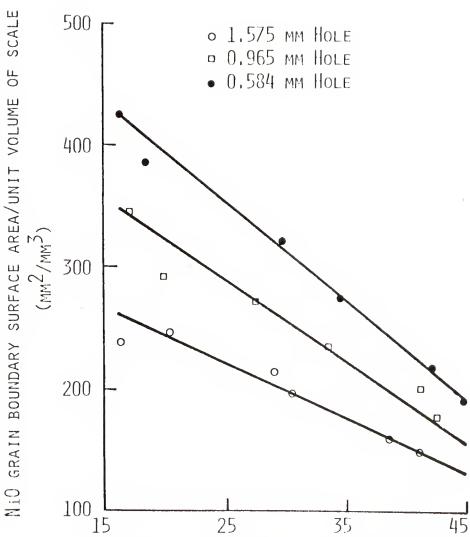

Figure 24. NiO grain boundary surface area per unit volume of scale, $S_{V\ TOTAL}$, versus total scale thickness, X, for hole specimens.

the earlier is the nucleation of new grains at the metal/oxide interface. It follows that the earlier the onset of NiO grain boundary sweeping, the larger is the equiaxed fraction of total scale thickness. Therefore, as the nickel surface curvature decreases, the equiaxed fraction of total scale thickness should increase. Figure 12 shows this behavior to exist at all oxidation times.

The columnarity of the outer layer is also affected by the onset of NiO grain boundary sweeping. The earlier NiO grain boundary sweeping beings, the thinner is the columnar layer developed during the initial stage of oxidation and the earlier is the lateral growth of NiO grains (which does not occur during the diffusion-controlled initial stage). It follows that the earlier the onset of NiO grain boundary sweeping, the smaller is the columnarity of the outer layer, $X_{COL}/\bar{X}_{COL}$. Therefore, as the nickel surface curvature decreases, the columnarity of the outer layer should also decrease. Experimental verification of this behavior is found in Figure 13 for all oxidation times.

4.1.4. The Geometric Effect of Nickel Surface Curvature

Oxidation of convex nickel surfaces (wires) results in a decrease in the metal/oxide interfacial area, whereas oxidation of concave nickel surfaces (holes) causes an increase in the metal/oxide interfacial area. These changes in the surface area through which nickel is transported suggest a change in the delivery of nickel into the scale.

Consequently, it may be argued that the effect of nickel surface curvature upon NiO scale thickening can be explained by specimen geometry alone.

To evaluate the effect of metal/oxide interfacial area upon the total scale thickness, the radius of the metal/oxide interface, $R_{M/O}$, was calculated for each condition of oxidation. The manner in which $R_{M/O}$ was computed is outlined in Figure 25 and the results recorded in Table XV. $R_{M/O}$ is directly proprotional to the metal/oxide interfacial area since $A_{M/O} = 2\pi R_{M/O} L$, where L is an assumed length of interface parallel to the cylindrical axis which is equal for all specimen geometries and remains constant during oxidation. Examination of Figure 26 reveals that the total NiO scale thickness increases linearly with decreasing $R_{M/O}$ (decreasing metal/oxide interfacial area) for wire specimens and with increasing $R_{M/O}$ for hole specimens. Thus, it would seem that specimen geometry, in so far as it affects the metal/oxide interfacial area, could explain the effect of nickel surface curvature upon the oxidation rate. That this possibility is not realized in fact, however, is demonstrated by comparing the volume of NiO scale generated with that which would have been formed under conditions of proportionality to the metal/oxide interfacial area. Thus, if one takes the product of the metal/oxide interfacial area and the total scale thickness, to obtain a volume that is proportional to the interfacial area, it will be obvious that this is not the same as the volume enclosed between the

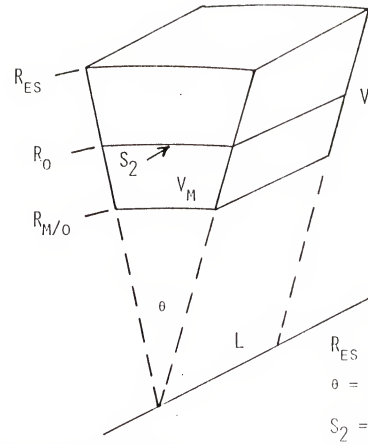

V_O - VOLUME OF OXIDE FORMED

V_M - VOLUME OF METAL CONSUMED

X - TOTAL SCALE THICKNESS IN MM.

R_{ES} - RADIUS OF THE EXTERNAL SURFACE IN MM.

R_O - ORIGINAL RADIUS OF SPECIMEN IN MM.

$R_{M/O}$ - RADIUS OF THE METAL/OXIDE INTERFACE IN MM.

$$V_M = \tfrac{1}{2}\theta(R_O^2 - R_{M/O}^2)L \qquad (1)$$

$$V_O = 1.6V_M = \tfrac{1}{2}\theta(R_{ES}^2 - R_{M/O}^2)L \qquad (2)$$

COMBINE EQUATIONS (1) AND (2) AND SOLVE FOR $R_{M/O}$

Figure 25. Method of calculating the radius of the metal/oxide interface, $R_{M/O}$.
(a) For wire specimens.

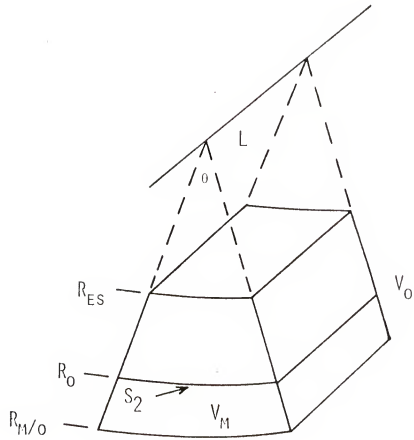

$R_{M/O} - R_{ES} = X$

$\theta = S_2/R_O$

$S_2 = 1x10^{-3}$ MM

$L = 1x10^{-3}$ MM

$$V_M = \tfrac{1}{2}\theta(R_{M/O}^2 - R_O^2)L \qquad (3)$$

$$V_O = 1.6V_M = \tfrac{1}{2}\theta(R_{M/O}^2 - R_{ES}^2)L \qquad (4)$$

COMBINE EQUATIONS (3) AND (4) AND SOLVE FOR $R_{M/O}$

Figure 25. (continued).
(b) For hole specimens.

Table XV

Radius of the Metal/Oxide Interface for Wire and Hole Nickel 270 Specimens

Specimen Diameter (mm)	Surface Curvature, 1/r (mm^{-1})	Oxidation Time (hours)	Total Scale Thickness, X ($\times 10^{-3}$ mm)	Radius of the Metal/Oxide Interface, $R_{M/O}$ ($\times 10^{-3}$ mm)
0.584 wire	3.42	4	8.33	286.7
0.965 wire	2.07	4	9.00	475.6
1.575 wire	1.27	4	10.07	781.2
1.575 hole	-1.27	4	16.53	797.9
0.965 hole	-2.07	4	17.08	492.9
0.584 hole	-3.42	4	16.32	302.0
0.584 wire	3.42	9	13.09	283.7
0.965 wire	2.07	9	14.05	473.4
1.575 wire	1.27	9	14.69	778.4
1.575 hole	-1.27	9	20.39	800.3
0.965 hole	-2.07	9	19.79	494.6
0.584 hole	-3.42	9	18.68	303.4

Table XV - Continued

Specimen Diameter (mm)	Surface Curvature, 1/r (mm^{-1})	Oxidation Time (hours)	Total Scale Thickness, X ($\times 10^{-3}$ mm)	Radius of the Metal/Oxide Interface, $R_{M/O}$ ($\times 10^{-3}$ mm)
0.584 wire	3.42	16	17.75	280.8
0.965 wire	2.07	16	18.71	469.6
1.575 wire	1.27	16	18.94	775.7
1.575 hole	-1.27	16	29.08	805.2
0.965 hole	-2.07	16	27.42	499.5
0.584 hole	-3.42	16	29.78	310.2
0.584 wire	3.42	25	19.05	279.9
0.965 wire	2.07	25	21.06	469.1
1.575 wire	1.27	25	23.57	772.8
1.575 hole	-1.27	25	30.61	806.2
0.965 hole	-2.07	25	33.53	503.5
0.584 hole	-3.42	25	34.75	313.2

Table XV - Continued

Specimen Diameter (mm)	Surface Curvature, 1/r (mm^{-1})	Oxidation Time (hours)	Total Scale Thickness, X ($\times 10^{-3}$ mm)	Radius of the Metal/Oxide Interface, $R_{M/O}$ ($\times 10^{-3}$ mm)
0.584 wire	3.42	36	22.58	277.7
0.965 wire	2.07	36	23.90	467.4
1.575 wire	1.27	36	27.01	770.6
1.578 hole	-1.27	36	38.81	811.5
0.965 hole	-2.07	36	41.03	507.4
0.584 hole	-3.42	36	42.02	317.5
0.584 wire	3.42	49	26.90	274.9
0.965 wire	2.07	49	28.56	464.6
1.575 wire	1.27	49	30.76	768.3
1.578 hole	-1.27	49	40.99	812.9
0.965 hole	-2.07	49	42.77	508.6
0.584 hole	-3.42	49	44.66	319.1

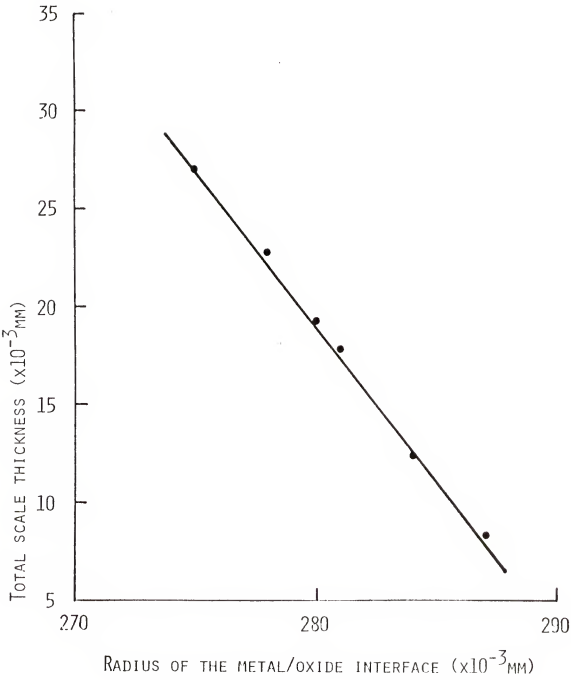

Figure 26. Total scale thickness, X, versus the radius of the metal/oxide interface, $R_{M/O}$.

(a) 0.584 mm diameter wire specimens.

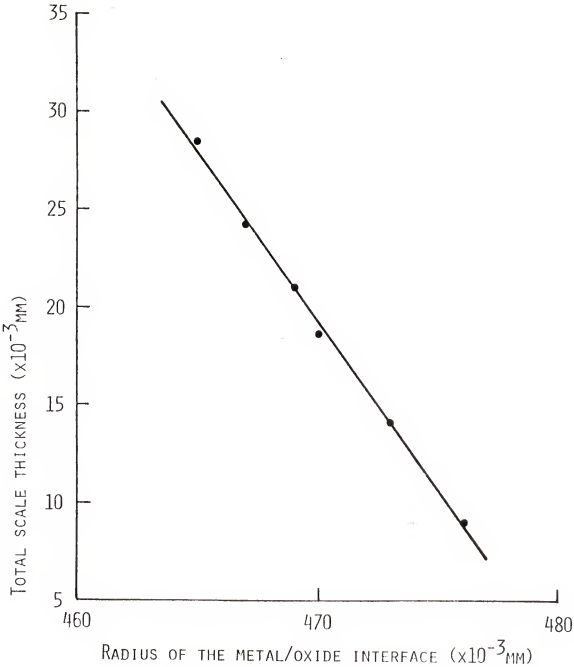

Figure 26. (continued).

(b) 0.965 mm diameter wire specimens.

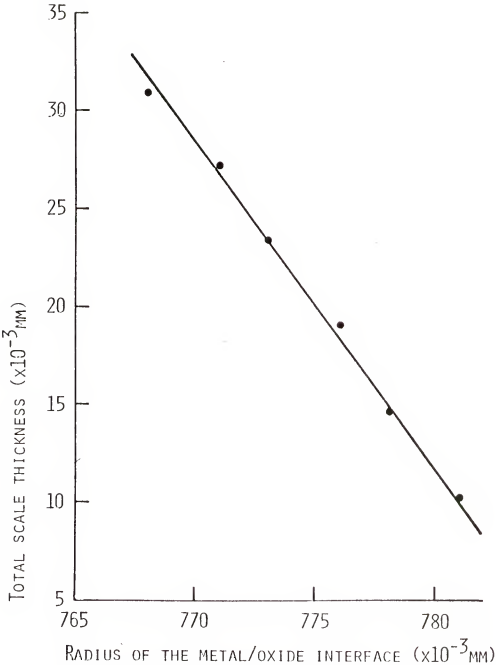

Figure 26. (continued).

(c) 1.575 mm diameter wire specimens.

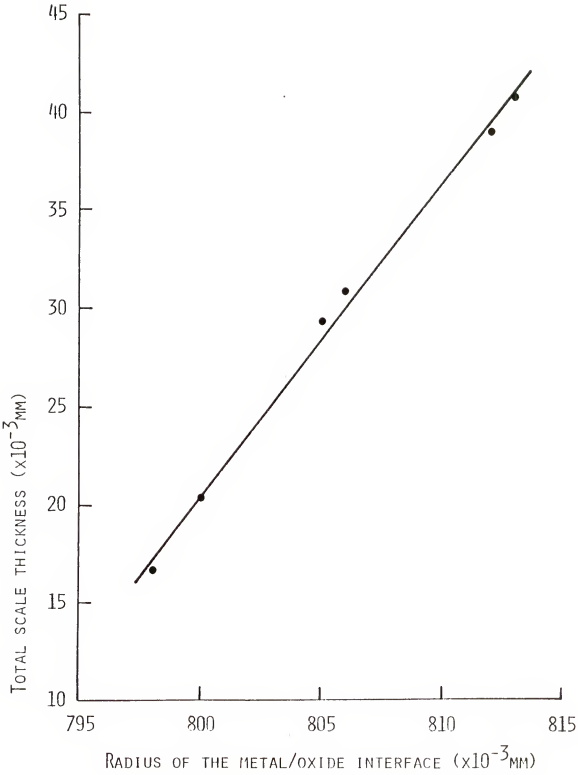

Figure 26. (continued).

(d) 1.575 mm diameter hole specimens.

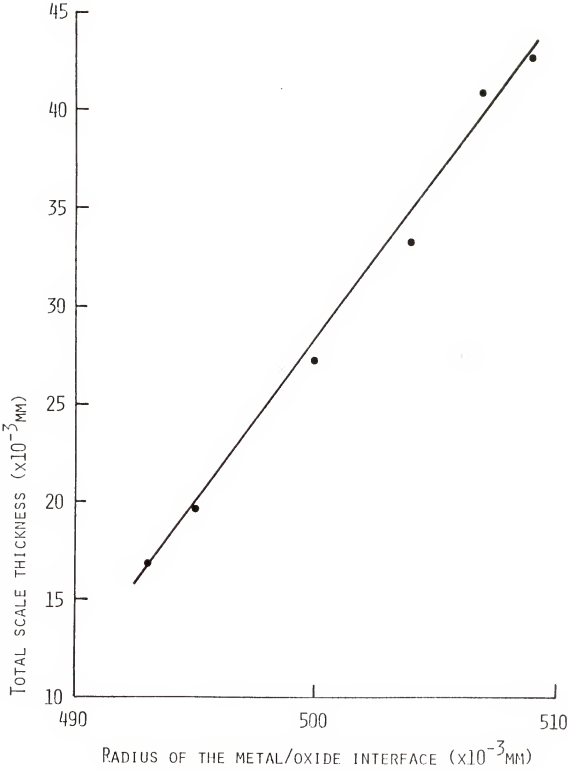

Figure 26. (continued).

(e) 0.965 mm diameter hole specimens.

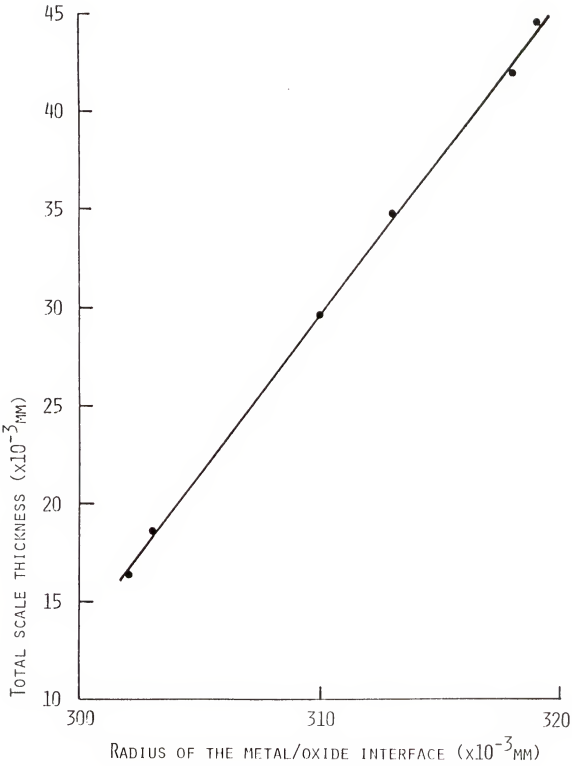

Figure 26. (continued).

(f). 0.584 mm diameter hole specimens.

metal/oxide interface and the corresponding external surface of the scale. In the case of convex surfaces (wires), the true volume is the larger; in the case of concave surfaces (holes), the true volume is the smaller, Figure 27.

Furthermore, specimen geometry, per se, cannot account for i) a larger NiO grain size upon hole specimens than upon wire specimens, ii) a linearly increasing relative thickness of the equiaxed layer to the total scale thickness with decreasing nickel surface curvature and iii) a linearly decreasing columnarity of the outer layer with decreasing nickel surface curvature. It is thought that these observations stem from the existence of a steady-state NiO grain growth process. The columnarity assumes the steady-state, which is characteristic of the nickel surface curvature, and it is developed and maintained in the following manner. Scale thickening proceeds without NiO grain growth until the columnar grains have attained a critical length to breadth ratio (i.e. columnarity, $\chi_{COL}/\bar{\chi}_{COL}$), whereupon the compressive stress generated within the scale is capable of deforming the entire structure. NiO grain boundary migration can then proceed, causing NiO grain growth and with it an accelerated rate of scale growth. This length to breadth ratio is maintained automatically, because, if the NiO grain growth were to proceed more rapidly than scale thickening, the NiO grains would return to a subcritical length to breadth ratio and grain growth would cease.

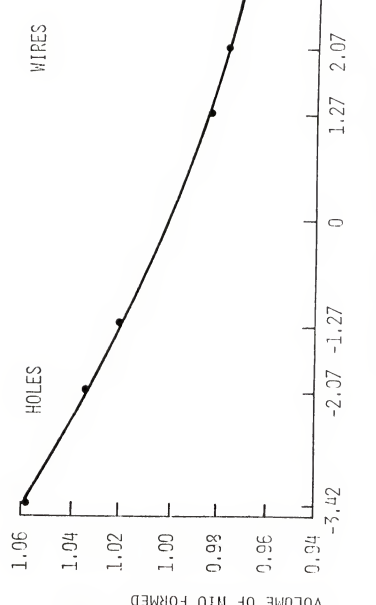

Figure 27. Ratio of calculated to true volume of NiO formed, V_C/V_T, versus nickel surface curvature, 1/r, for 25 hours of oxidation.

If, however, scale growth were to proceed too rapidly, an excess of compressive stress would be generated and cause an acceleration of NiO grain growth, until a balance was re-established.

4.2. The Effect of Oxidation Temperature Upon the High-Temperature Oxidation of Nickel

Oxidation of Nickel 270 flat specimens at 1000°C and 800°C has yielded the following results:

1. All scale thickening curves intersect the oxidation time axis at positive values, the 1000°C curves having a larger value of intersection than the corresponding 800°C curves.
2. The total NiO scale thickness is larger upon flat specimens oxidized at 1000°C than upon those oxidized at 800°C.
3. The NiO grain size is larger upon flat specimens oxidized at 1000°C than upon those oxidized at 800°C.
4. The relative thickness of the equiaxed layer to the total scale thickness, X_{EQ}/X, is larger upon flat specimens oxidized at 800°C than upon those oxidized at 1000°C.

These results are consistent with the proposed model of the high-temperature oxidation of nickel (section 4.1.1.).

4.2.1. The Effect of Oxidation Temperature Upon the Proposed Model

Oxidation temperature also affects the proposed model of oxidation by controlling the onset of NiO grain boundary sweeping (later stage of oxidation). It is expected that the oxidation temperature affects the plasticity of NiO. The lower the oxidation temperature, the less plastic is the NiO scale and the greater is the restraint to outward extrusion of newly formed NiO along oxide grain boundaries, for a given scale thickness. Thereby, a greater force is exerted upon neighboring NiO grains at 800°C. Consequently, the onset of NiO grain boundary sweeping and nucleation of new NiO grains at the metal/oxide interface occurs earlier in oxidation the lower the oxidation tempeature.

Graphical support of this effect is found in Figures 18 and 19, total scale thickness and columnar layer thickness, respectively, versus oxidation time for flat specimens oxidized at 1000°C and 800°C. These curves show the intersection with the oxidation time axis to have a larger value for 1000°C oxidation than for 800°C oxidation. As before, these intersections correspond to point A in Figure 20, the schematic representation of oxidation, and estimate the time during which diffusion-controlled growth of NiO occurs (initial stage) and before which NiO grain boundary sweeping begins (later stage). The value of these intercepts is shown as incubation time in Tables XVI and XVII, as calculated from the kinetic equations for total scale thickness and

Table XVI

Incubation Times for NiO Grown Upon Flat Nickel 270 Specimens Calculated From Total Scale Thickness Data

Specimen Oxidation Temperature (°C)	Incubation Time (hours)
1000	1.56×10^{-1}
800	6.20×10^{-2}

Table XVII

Incubation Times for NiO Grown Upon Flat Nickel 270 Specimens Calculated From Columnar Layer Thickness Data

Specimen Oxidation Temperature (°C)	Incubation Time (hours)
1000	1.59×10^{-1}
800	1.15×10^{-1}

columnar layer thickness, respectively. In each case, the lower oxidation temperature (800°C) corresponds to the shorter incubation time. Thus, oxidation temperature controls the onset of NiO grain boundary sweeping. The lower the oxidation temperature, the earlier is the onset of NiO grain boundary sweeping.

Again, care should be taken not to associate the incubation times with the moment of onset of NiO grain boundary sweeping. Since the NiO scale thickening curves were extrapolated to zero oxidation time, these values merely indicate that NiO grain boundary sweeping begins earlier as oxidation temperature is lowered.

4.2.2. The Effect of Oxidation Temperature Upon the Scale Thickening and Microstructural Evolution of NiO

Because the diffusion rates of the reactants and the rate of NiO grain boundary sweeping are faster at 1000°C than at 800°C, a thick, coarse-grained oxide develops at 1000°C compared to a thin, fine-grained oxide at 800°C, Figure 6. These physical properties of the NiO scale exist despite the earlier onset of NiO grain boundary sweeping at 800°C, which, all conditions being equal, would dictate a thicker, coarser-grained oxide than that formed at 1000°C.

The relative thickness of scale layers is determined solely by the onset of NiO grain boundary sweeping. The earlier NiO grain boundary sweeping begins, the thinner is the columnar layer developed during the initial stage of

oxidation and the earlier is the nucleation of new grains at the metal/oxide interface. It follows that the earlier the onset of NiO grain boundary sweeping, the larger is the equiaxed fraction of total scale thickness. Therefore, as the oxidation temperature is lowered, the equiaxed fraction of total scale thickness should increase. Figure 17 confirms this trend at all oxidation times.

CHAPTER V

CONCLUSIONS

1. The high-temperature oxidation of nickel is a two-stage process. The initial stage is controlled by diffusion of the reactants and the later stage by NiO grain boundary sweeping.
2. Nickel surface curvature affects the lateral, compressive stresses generated within the NiO scale during oxidation, thereby controlling the duration of each stage.
3. The incubation time before the onset of NiO grain boundary sweeping (later stage of oxidation) decreases as nickel surface curvature decreases.
4. An earlier onset of NiO grain boundary sweeping with decreasing nickel surface curvature causes: i) the total scale thickness to increase; ii) the relative thickness of the equiaxed layer to the total scale thickness to increase; and iii) the columnarity of the outer layer to decrease.
5. NiO grain growth occurring concurrently with NiO scale growth results in coarser-grained oxide scales upon hole specimens (thicker oxide scales) than upon wire specimens (thinner oxide scales).

6. An uncontrolled difference in the basic grain size between wire and hole specimens exists, yielding a refinement in the initial NiO grain size upon hole specimens. Presumably, this difference results from an effect of nickel surface curvature upon the oxygen gas flow.
7. Total scale thickness is proportional to nickel surface curvature, which in turn, is proportional to the metal/oxide interfacial area; however, neither is proportional to the volume of NiO scale formed. For convex surfaces (wires), the volume of scale formed is greater than the product of total scale thickness and metal/oxide interfacial area, and for concave surfaces (holes), the volume of scale formed is less than this product.
8. Oxidation temperature affects the plasticity of the NiO scale, thereby controlling the duration of each stage of oxidation.

APPENDICES

APPENDIX I

EQUIAXED LAYER THICKNESS DATA FOR WIRE, HOLE AND FLAT SPECIMENS

Table I-1

Equiaxed Layer Thickness Measurements for Wire and Hole Nickel 270 Specimens

Specimen Diameter (mm)	Surface Curvature, $1/r$ (mm^{-1})	Oxidation Time (hours)	Equiaxed Layer Thickness, X_{EQ} ($\times 10^{-3}$ mm)
0.584 wire	3.42	4	3.41 ± 0.18
0.965 wire	2.07	4	4.01 ± 0.23
1.575 wire	1.27	4	4.53 ± 0.33
1.575 hole	-1.27	4	6.08 ± 0.38
0.965 hole	-2.07	4	8.07 ± 0.39
0.584 hole	-3.42	4	8.52 ± 0.32
0.584 wire	3.42	9	4.37 ± 0.25
0.965 wire	2.07	9	5.10 ± 0.22
1.575 wire	1.27	9	5.56 ± 0.22
1.575 hole	-1.27	9	8.56 ± 0.38
0.965 hole	-2.07	9	9.16 ± 0.43
0.584 hole	-3.42	9	9.94 ± 0.35

Table 1-1 - Continued

Specimen Diameter (mm)	Surface Curvature, $1/r$ (mm^{-1})	Oxidation Time (hours)	Equiaxed Layer Thickness, X_{EQ} ($\times 10^{-3}$ mm)
0.584 wire	3.42	16	5.54 ± 0.28
0.965 wire	2.07	16	6.16 ± 0.29
1.575 wire	1.27	16	6.94 ± 0.30
1.575 hole	-1.27	16	12.44 ± 0.53
0.965 hole	-2.07	16	13.41 ± 0.56
0.584 hole	-3.42	16	15.92 ± 0.75
0.584 wire	3.42	25	7.02 ± 0.33
0.965 wire	2.07	25	7.63 ± 0.31
1.575 wire	1.27	25	8.62 ± 0.32
1.575 hole	-1.27	25	13.77 ± 0.46
0.965 hole	-2.07	25	16.09 ± 0.78
0.584 hole	-3.42	25	18.50 ± 0.58

Table I-1 - Continued

Specimen Diameter (mm)	Surface Curvature, $1/r$ (mm^{-1})	Oxidation Time (hours)	Equiaxed Layer Thickness, X_{EQ} ($\times 10^{-3}$ mm)
0.584 wire	3.42	36	8.30 ± 0.28
0.965 wire	2.07	36	9.36 ± 0.23
1.575 wire	1.27	36	11.05 ± 0.27
1.575 hole	-1.27	36	17.24 ± 0.71
0.965 hole	-2.07	36	20.10 ± 0.77
0.584 hole	-3.42	36	22.00 ± 0.61
0.584 wire	3.42	49	9.50 ± 0.43
0.965 wire	2.07	49	11.48 ± 0.45
1.575 wire	1.27	49	12.99 ± 0.57
1.575 hole	-1.27	49	18.86 ± 0.83
0.965 hole	-2.07	49	20.94 ± 0.92
0.584 hole	-3.42	49	23.68 ± 0.92

Table I-2

Equiaxed Layer Thickness Measurements for Flat Nickel 270 Specimens

Specimen Oxidation Temperature (°C)	Oxidation Time (hours)	Equiaxed Layer Thickness, X_{EQ} ($\times 10^{-3}$ mm)
1000	4	4.14 ± 0.32
800	4	--
1000	9	6.10 ± 0.37
800	9	4.69 ± 0.30
1000	16	8.20 ± 0.51
800	16	5.49 ± 0.34
1000	25	8.24 ± 0.45
800	25	6.85 ± 0.34
1000	36	10.48 ± 0.76
800	36	7.55 ± 0.34
1000	49	10.81 ± 0.72
800	49	8.28 ± 0.34

APPENDIX II

COMPUTATION OF THE "CALCULATED" TOTAL SCALE THICKNESS FOR THE NiO FORMED UPON CURVED SPECIMENS

The "calculated" curves present in Figures 7 and 8 (total scale thickness versus oxidation time for wire and hole specimens, respectively) represent the total thickness of NiO which should form upon the particular specimen based on geometric considerations and assuming flat specimen kinetics are operating at the 1000°C oxidation temperature. The manner in which these curves were derived is illustrated in Figures II-1 and II-2. An oxide scale depth (normal to the plane of the figure) of 1 mm is assumed allowing the difference in densities, ρ, between nickel and nickel oxide, $\rho_{Ni} = 0.625\ _{NiO}$, to be used in equations (1) and (7). The factor $1/2\pi R$ of equations (2), (4), (8) and (10) normalizes the oxide per unit length. Total scale thickness, taken from Table IX for flat Nickel 270 specimens oxidized at 1000°C, is substituted for A_o in equations (3), (5), (9) and (11). Values for R_o and R_I are obtained, and the "calculated" total scale thickness may then be found from equations (6) and (12).

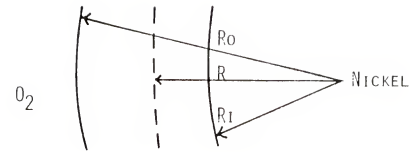

An - Area of nickel consumed
Ao - Area of NiO formed
Ro - Radius of wire plus oxide after oxidation
R - Original radius of wire
Ri - Radius of wire after oxidation
X - Thickness of NiO formed

$$An = 0.625\ Ao \quad (1)$$

$$An = \pi(R^2 - Ri^2)\frac{1}{2\pi R} \quad (2)$$

$$Ri = [R^2 - 2R\ (0.625)\ Ao]^{1/2} \quad (3)$$

$$Ao = \pi(Ro^2 - Ri^2)\frac{1}{2\pi R} \quad (4)$$

$$Ro = (2RAo + Ri^2)^{1/2} \quad (5)$$

$$X = Ro - Ri \quad (6)$$

Figure II-1. Method of determining the "calculated" total scale thickness, $X = R_o - R_I$, of NiO formed upon wire specimens.

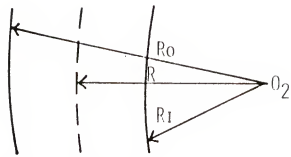

AN - AREA OF NICKEL CONSUMED
AO - AREA OF NiO FORMED
RO - RADIUS OF HOLE PLUS OXIDE AFTER OXIDATION
R - ORIGINAL RADIUS OF HOLE
RI - RADIUS OF HOLE AFTER OXIDATION
X - THICKNESS OF NiO FORMED

$$A_N = 0.625\ A_O \tag{7}$$

$$A_N = \pi(R_O^2 - R^2)\frac{1}{2\pi R} \tag{8}$$

$$R_O = [2R\ (0.625)\ A_O + R^2]^{1/2} \tag{9}$$

$$A_O = \pi(R_O^2 - R_I^2)\frac{1}{2\pi R} \tag{10}$$

$$R_I = (R_O^2 - 2RA_O)^{1/2} \tag{11}$$

$$X = R_O - R_I \tag{12}$$

Figure II-2. Method of determining the "calculated" total scale thickness, $X = R_O - R_I$, of NiO formed upon hole specimens.

BIBLIOGRAPHY

[1] Y. Iida, S. Ozaki and K. Shimada, Rep. Gov. Indust. Research Inst. Nagoya, 6, 569 (1957).

[2] P. Hancock and R. Fletcher, ATB Métallurgie, 6, 1 (1966).

[3] J. Romanski, Corrosion Science, 8, 67 (1968).

[4] J. Romanski, Corrosion Science, 8, 89 (1968).

[5] A. V. Borovski, V. M. Vasutneski and G. N. Kartmasov, Zashchita Metallov, 6, 352 (1970).

[6] J. A. Sartell and C. H. Li, J. Inst. Metals, 90, 92 (1961).

[7] T. Ueno, Trans. Jap. Inst. Metals, 15, 167 (1974).

[8] R. T. Phelps, E. A. Gulbransen and J. W. Hickman, Indust. Eng. Chem. Analyt. Ed., 18, 391 (1946).

[9] A. Dravnieks and H. J. McDonald, J. Electrochem. Soc., 94, 139 (1948).

[10] S. Mrowec, Corrosion Science, 7, 563 (1967).

[11] B. M. Vasyutinsky and G. N. Kartmazov, Physics Metals Metallography, 15, 120 (1963).

[12] G. C. Wood and I. G. Wright, Corrosion Science, 5, 841 (1965).

[13] I. A. Menzie and P. Aldred, Corrosion Science, 8, 525 (1968).

[14] J. Païdassi and L. Berry, Metaux-Corrosion-Inds., 44, 129 (1969).

[15] J. Maldy, Compt. Pend. Acad. Sci. Paris, 258, 1500 (1964).

[16] F. N. Rhines and J. S. Wolf, Met. Trans., 1, 1701 (1970).

[17] O. A. Pashkova, H. P. Zhuk, B. K. Opara and N. I. Burtseva, Zashita Metallov, 6, 591 (1970).

[18] F. N. Rhines and R. G. Connell, Jr., Stress Effects and the Oxidation of Metals, Ed. by J. V. Cathcart, 1974 Fall Meeting TMS-AIME, p. 94.

[19] F. N. Rhines and R. G. Connell, Jr., J. Electrochem. Soc., 124, 1122 (1977).

[20] V. I. Arkharvo, S. I. Ivanovskaya and A. S. Krivonosova, Physics Metals Metallography, 22, 75 (1966).

[21] A. Preece and G. Lucas, J. Inst. Metals, 81, 219 (1952).

[22] R. Herchl, N. N. Khoi, T. Homma and W. W. Smeltzer, Oxidation of Metals, 4, 35 (1972).

[23] R. Hales and H. C. Hill, Corrosion Science, 12, 843 (1972).

[24] A. G. Evans, Rajdev and D. L. Douglas, Oxidation of Metals, 4, 151 (1972).

[25] R. J. Hussey, P. E. Beaubien and D. Caplan, Metallography, 16, 27 (1973).

[26] L. B. Pfeil, J. Iron and Steel Inst., 119, 501 (1929).

[27] J. M. Perrow, W. W. Smeltzer and R. K. Ham, Acta Met., 15, 577 (1967).

[28] J. M. Perrow, W. W. Smeltzer and J. D. Embury, Acta Met., 16, 1209 (1968).

[29] M. J. Graham, D. Caplan and M. Cohen, J. Electrochem. Soc., 119, 1265 (1972).

[30] R. F. Tylecote, J. Iron and Steel Inst., 196, 135 (1960).

[31] J. Païdassi, Third Colloque de Métallurgie sur la Corrosion, Saclay 1959, p. 171.

[32] M. W. Vernon and F. J. Spooner, J. Mat. Sci., 4, 112 (1969).

[33] D. Bruce and P. Hancock, J. Inst. Metals, 97, 140 (1969).

[34] D. Bruce and P. Hancock, J. Inst. Metals, 97, 148 (1969).

[35] M. T. Shim and W. J. Moore, J. Phys. Chem., 26, 802 (1957).

[36] J. S. Choi and W. J. Moore, J. Phys. Chem., 66, 1308 (1962).

[37] R. Linder and A. Akerstrom, Discuss. Faraday Soc., 23, 133 (1957).

[38] M. O'Keefe and W. J. Moore, J. Phys. Chem., 65, 1438 (1961).

[39] M. L. Volpe and J. Reddy, J. Phys. Chem., 53, 1117 (1970).

[40] M. Kuise, Angew. Elektrochemie, 9, 318 (1971).

[41] Y. Oshi and W. D. Kingery, J. Phys. Chem., 33, 480 (1960).

[42] F. J. Wilkins and E. K. Rideal, Proc. Roy. Soc., A, 128 (1930).

[43] W. J. Moore, Y. Ebisuzaki and J. A. Sluss, Z. Elektrochemie, 62, 1438 (1958).

[44] H. Hashimoto and M. Hama, J. Appl. Phys., 43, 4828 (1972).

[45] D. Caplan and G. I. Sproule, Oxidation of Metals, 9, 459 (1975).

[46] B. Illschner and H. Pfeiffer, Naturwiss., 40, 603 (1953).

[47] S. Mrowec and T. Werber, Acta Met., 8, 819 (1960).

[48] U. R. Evans, J. Chem. Soc., II, 1020 (1927).

[49] P. D. Dankov and P. V. Churaev, Doklady Akad. Nauk. SSSR, 73, 1221 (1950).

[50] D. B. Dove and D. H. Baldwin, Met. Trans., 5, 1637 (1974).

[51] E. T. Denisenko and V. V. Skorokhod, Poroshkovaya Met., 4, 83 (1972).

[52] A. Norin, Oxidation of Metals, 9, 259 (1975).

[53] J. V. Cathcart, R. E. Pawel and G. F. Petersen, High Temperature Oxidation of Uranium Alloys, Internat. Corrosion Conference, Tokyo, June 1972.

[54] W. K. Appleby and R. F. Tylecote, Corrosion Science, 10, 325 (1970).

[55] T. Homma and S. Issika, Acta Met., 12, 1092 (1964).

[56] R. E. Pawel, J. V. Cathcart and J. J. Campbell, J. Electrochem. Soc., 110, 551 (1963).

[57] L. J. Weirick and W. L. Larsen, J. Electrochem. Soc. Solid State Science and Technology, 119, 465 (1972).

[58] R. Hales, Corrosion Science, 12, 555 (1972).

[59] J. V. Cathcart, G. F. Petersen and C. J. Sparks, Jr., J. Electrochem. Soc., 116, 664 (1969).

[60] J. E. Antill and J. B. Washburn, J. Electrochem. Soc., 114, 1215 (1967).

[61] J. Maldy, Commissariat á l'Energie Atomique 7th Colloque de Métallurgie, Saclay, 1963, p. 71.

[62] F. Robin, Bull. de al Société de Encouragement, CXVIII, 204 (1912).

[63] U. M. Martins, Canadien J. Phys, 33, 466 (1955).

[64] M. G. Lozinsky and E. I. Antipova, Metallovedenie i Term. Obrabot. Metallov, 11, 18 (1962).

[65] G. C. Wood and B. Chattopadhyay, Corrosion Science, 10, 471 (1970).

[66] P. H. Holloway and J. B. Hudson, Surface Science, 43, 123 (1974).

[67] E. A. Gulbransen, Corrosion, 12, 61 (1956).

[68] D. Caplan, M. J. Graham and M. Cohen, J. Electrochem. Soc. Solid State Science and Technology, 119, 1205 (1972).

[69] E. A. Gulbransen and K. F. Andrew, J. Electrochem. Soc., 101, 128 (1954).

[70] E. S. Karakozov, I. N. Shabalin and A. A. Schmykov, Fizika i Khim Obrabot. Mat., 4, 151 (1970).

[71] M. J. Graham, G. I. Sproule, D. Caplan and M. Cohen, J. Electrochem. Soc., 119, 883 (1972).

[72] J. B. Newkirk and W. G. Marin, Trans. Met. Soc. AIME, 212, 398 (1958).

[73] C. A. Papageorgopoulous and J. M. Chen, Solid State Commun., 13, 1455 (1 Nov. 1973).

[74] J. R. Anderson and I. M. Ritchie, Proc. Roy. Soc., A, 299, 354 (1967).

[75] K. M. Carlsen, Acta Met., 5, 58 (1957).

[76] M. J. Graham, R. J. Hussey and M. Cohen, J. Electrochem. Soc., 120, 1523 (1973).

[77] G. Tammann, Z. Anorg. Chemie, 111, 78 (1920).

[78] G. Tammann and W. Köster, Z. Anorg U. Allg. Chemie, 123, 196 (1922).

[79] G. Tammann and C. F. Marais, Z. Anorg. Chemie, 135, 127 (1924).

[80] J. S. Dunn, Proc. Roy. Soc., A, 111, 203 (1926).

[81] G. Tammann and K. Bochow, Z. Anorg. Chemie, 169, 42 (1928).

[82] F. H. Constable, Proc. Roy. Soc., A, 117, 376 (1928).

[83] C. Wagner and K. Grunewald, Z. Physikal. Chem., B. 40, 455 (1938).

[84] D. J. McAdam, Jr. and G. W. Geil, J. Research Nat. Bur. Stds., 28, 593 (1942).

[85] E. S. Vorontsov and V. D. Suikovskaya, Izuest. Akad. Nauk. SSSR, 4, 226 (1970).

[86] K. Hauffe, L. Pethe, R. Schmidt and S. R. Morrison, J. Electrochem. Soc., 115, 456 (1966).

[87] J. C. Rocaries and M. Rigaud, Scripta Met., 5, 59 (1971).

[88] J. M. Ritchie, Phil. Mag., 19, 421 (1969).

[89] M. J. Graham and M. Cohen, J. Electrochem. Soc., 119, 879 (1972).

[90] N. B. Philling and R. E. Bedworth, J. Inst. Metals, 29, 529 (1923).

[91] G. Valensi, Compt. Rend., 201, 523 (1935).

[92] J. A. Sartell, R. J. Stokes, S. H. Bendel, T. L. Johnson and C. H. Li, Trans. AIME, 215, 420 (1959).

[93] J. C. Bokros and W. R. Wallace, Corrosion, 16, 117 (1960.

[94] L. Berry and J. Païdassi, Compt. Rend., 255, 2253 (1962).

[95] F. S. Petit and E. J. Felton, J. Electrochem. Soc., 111, 135 (1964).

[96] J. D. Christian and W. P. Gilbreath, Oxidation of Metals, 9, 1 (1975).

[97] G. C. Wood, I. G. Wright and J. M. Ferguson, Corrosion Science, 5, 645 (1965).

[98] C. Wagner, Z. Phys. Chem., B21, 25 (1933).

[99] D. L. Douglass, Materials, 1 (1971).

[100] K. Fueki and J. B. Wagner, Jr., J. Electrochem. Soc., 112, 384 (1965).

[101] T. G. Kravchenko, E. A. Shelement'eva, N. P. Zhuk and G. P. Karpman, Zashchita Metallov, 2, 312 (1966).

[102] J. J. van den Brock and J. L. Meijering, Acta Meta., 16, 375 (1968).

[103] W. E. Campbell and U. B. Thomas, Trans. Electrochem. Soc., 91, 623 (1947).

[104] F. N. Rhines, Met. Trans., 1, 1105 (1970).

[105] J. A. Holbrook, Control of Environmental Surface Reactions, Diffusion Transport, Final Report, NSF Grant GH-34550, 1973, p. 47.

BIOGRAPHICAL SKETCH

H. John Healey, Jr. was born on June 25, 1951 in Orange, New Jersey. He received his elementary education in the public schools of Bloomfield, New Jersey and was graduated from Glen Ridge High School, Glen Ridge, New Jersey, in 1969. Between 1969 and 1973 he attended Lafayette College in Easton, Pennsylvania, where he received the degree of Bachelor of Science in Metallurgical Engineering in 1973. In the Fall of 1973 he entered the University of Florida Graduate School in the Department of Materials Science and Engineering. During the next four and one-half years he pursued studies and research leading toward the degree of Doctor of Philosophy, which he received in 1978.

The author is married to the former Dianne Cipolla of Hollywood, Florida. He is a member of the American Institute of Mining, Metallurgical and Petroleum Engineers, American Society for Metals, National Association of Corrosion Engineers, Phi Beta Kappa, Tau Beta Pi, and Alpha Sigma Mu.

I certify that I have read this study and that in my opinion it conforms to acceptable standards of scholarly presentation and is fully adequate, in scope and quality, as a dissertation for the degree of Doctor of Philosophy.

Frederick N. Rhines, Chairman
Distinguished Service Professor
of Materials Science and
Engineering

I certify that I have read this study and that in my opinion it conforms to acceptable standards of scholarly presentation and is fully adequate, in scope and quality, as a dissertation for the degree of Doctor of Philosophy.

Ellis D. Verink, Jr.
Professor and Chairman of Materials Science and Engineering

I certify that I have read this study and that in my opinion it conforms to acceptable standards of scholarly presentation and is fully adequate, in scope and quality, as a dissertation for the degree of Doctor of Philosophy.

Robert T. DeHoff
Professor of Materials Science
and Engineering

I certify that I have read this study and that in my opinion it conforms to acceptable standards of scholarly presentation and is fully adequate, in scope and quality, as a dissertation for the degree of Doctor of Philosophy.

James E. Keesling
Professor of Mathematics

This dissertation was submitted to the Graduate Faculty of the College of Engineering and to the Graduate Council, and was accepted as partial fulfillment of the requirements for the degree of Doctor of Philosophy.

June, 1978

Hubert O. Lewis
Dean, College of Engineering

Dean, Graduate School